

GLOBAL CHARACTERISTICS OF X-RAY FLASHES AND X-RAY–RICH GAMMA-RAY BURSTS OBSERVED BY *HETE*-2

T. SAKAMOTO,^{1,2,3} D. Q. LAMB,⁴ N. KAWAI,^{1,2} A. YOSHIDA,^{2,5} C. GRAZIANI,⁴ E. E. FENIMORE,⁶ T. Q. DONAGHY,⁴
 M. MATSUOKA,⁷ M. SUZUKI,¹ G. RICKER,⁸ J.-L. ATTEIA,⁹ Y. SHIRASAKI,¹⁰ T. TAMAGAWA,² K. TORII,¹¹
 M. GALASSI,⁶ J. DOTY,⁸ R. VANDERSPEK,⁸ G. B. CREW,⁸ J. VILLASENOR,⁸ N. BUTLER,⁸ G. PRIGOZHIN,⁸
 J. G. JERNIGAN,¹² C. BARRAUD,⁹ M. BOER,¹³ J.-P. DEZALAY,¹³ J.-F. OLIVE,¹³ K. HURLEY,¹²
 A. LEVINE,⁸ G. MONNELLY,⁸ F. MARTEL,⁸ E. MORGAN,⁸ S. E. WOOSLEY,¹⁴
 T. CLINE,³ J. BRAGA,¹⁵ R. MANCHANDA,¹⁶ G. PIZZICHINI,¹⁷
 K. TAKAGISHI,¹⁸ AND M. YAMAUCHI¹⁸

Received 2004 September 7; accepted 2005 April 15

ABSTRACT

We describe and discuss the global properties of 45 gamma-ray bursts (GRBs) observed by *HETE*-2 during the first 3 years of its mission, focusing on the properties of X-ray flashes (XRFs) and X-ray–rich GRBs (XRRs). We find that the numbers of XRFs, XRRs, and GRBs are comparable, and that the durations and the sky distributions of XRFs and XRRs are similar to those of GRBs. We also find that the spectral properties of XRFs and XRRs are similar to those of GRBs, except that the values of the peak energy $E_{\text{peak}}^{\text{obs}}$ of the burst spectrum in νF_{ν} , the peak energy flux F_{peak} , and the energy fluence S_E of XRFs are much smaller (and those of XRRs are smaller) than those of GRBs. Finally, we find that the distributions of all three kinds of bursts form a continuum in the [S_E (2–30 keV), S_E (30–400) keV] plane, the [S_E (2–400 keV), E_{peak}] plane, and the [F_{peak} (50–300 keV), E_{peak}] plane. These results provide strong evidence that all three kinds of bursts arise from the same phenomenon.

Subject heading: gamma rays: bursts

1. INTRODUCTION

Gamma-ray bursts (GRBs) whose energy fluences S_X in the X-ray energy band (2–30 keV) are larger than their energy fluences S_γ in the gamma-ray energy band (30–400 keV) have received increasing attention over the last few years. In particular, the Wide Field Camera (WFC) on *BepoSAX* detected

events that were not detected by the Gamma-Ray Burst Monitor (GRBM) on the same satellite. These events have been termed “X-ray flashes” (XRFs; Heise et al. 2001). Throughout this paper, we define “X-ray–rich” GRBs (XRRs) and XRFs as those events for which $\log [S_X(2–30 \text{ keV})/S_\gamma(30–400 \text{ keV})] > -0.5$ and >0.0 , respectively. While arbitrary, these definitions are independent of the properties of any instrument (they can therefore be used by anyone), and the definition of XRFs that we have adopted closely matches the instrument-dependent criterion introduced by Heise et al. (2001) for this kind of burst. Understanding the relationship between XRFs, XRRs, and GRBs may provide a deeper understanding of the prompt emission of GRBs.

2. OBSERVATIONS

In this paper, we investigate the global properties of a sample of the *High Energy Transient Explorer* 2 (*HETE*-2) bursts. We require the bursts in this sample to satisfy the following criteria: (1) the burst is detected in the Wide-Field X-Ray Monitor (WXM), (2) the burst is localizable by the WXM, and (3) the signal-to-noise ratio of the WXM data is sufficient to carry out a spectral analysis of the burst. Generally, a joint spectral analysis is carried out for the WXM and the French Gamma Telescope (FREGATE) data. Forty-five bursts observed by *HETE*-2 between the beginning of the *HETE*-2 mission and 2003 September 13 met these criteria, and this is the sample of bursts that we study.

An important question to consider is the degree to which this sample of bursts may be affected by observational selection effects. A key feature of GRBs (and XRFs and XRRs) is that their spectra are adequately fit by the Band spectral model, which consists of a power-law times exponential cutoff model with a cutoff energy of E_0 and a simple power law that smoothly joins at the so-called “break energy,” E_{break} (Band et al. 1993). The value of the low-energy power-law index α is typically in the range of -0.5 to -2 , and the value of the high-energy power-law index β

¹ Department of Physics, Tokyo Institute of Technology, 2-12-1 Ookayama, Meguro-ku, Tokyo 152-8551, Japan.

² RIKEN (Institute of Physical and Chemical Research), 2-1 Hirosawa, Wako, Saitama 351-0198, Japan.

³ NASA Goddard Space Flight Center, Greenbelt, MD, 20771.

⁴ Department of Astronomy and Astrophysics, University of Chicago, Chicago, IL, 60637.

⁵ Department of Physics, Aoyama Gakuin University, Chitosedai 6-16-1, Setagaya-ku, Tokyo 157-8572, Japan.

⁶ Los Alamos National Laboratory, P.O. Box 1663, Los Alamos, NM 87545.

⁷ Tsukuba Space Center, National Space Development Agency of Japan, Tsukuba, Ibaraki 305-8505, Japan.

⁸ Center for Space Research, Massachusetts Institute of Technology, 70 Vassar Street, Cambridge, MA 02139.

⁹ Laboratoire d’Astrophysique, Observatoire Midi-Pyrénées, 14 Avenue Edouard Belin, 31400 Toulouse, France.

¹⁰ National Astronomical Observatory, Osawa 2-21-1, Mitaka, Tokyo 181-8588, Japan.

¹¹ Department of Earth and Space Science, Graduate School of Science, Osaka University, 1-1 Machikaneyama-cho, Toyonaka, Osaka 560-0043, Japan.

¹² Space Sciences Laboratory, University of California, Berkeley, CA 94720-7450.

¹³ Centre d’Etude Spatiale des Rayonnements, CNRS/UPS, B.P. 4346, 31028 Toulouse Cedex 4, France.

¹⁴ Department of Astronomy and Astrophysics, 477 Clark Kerr Hall, University of California, Santa Cruz, CA 95064.

¹⁵ Instituto Nacional de Pesquisas Espaciais, Avenida Dos Astronautas 1758, São José dos Campos 12227-010, Brazil.

¹⁶ Department of Astronomy and Astrophysics, Tata Institute of Fundamental Research, Homi Bhabha Road, Mumbai 400 005, India.

¹⁷ INAF/IASF Sezione di Bologna, via Gobetti 101, 40129 Bologna, Italy.

¹⁸ Faculty of Engineering, Miyazaki University, Gakuen Kibanadai Nishi, Miyazaki 889-2192, Japan.

The distribution of the fluence ratio $S_x/(S_x - 30 \text{ keV})$ for the 45 bursts in this study is shown in Figure 2. The boundaries between GRBs and XRRs, and XRRs and XRFs, are shown as dashed lines. The figure clearly shows that XRFs, XRRs, and GRBs form a single broad distribution. The numbers of XRFs, XRRs, and GRBs, are 16, 19, and 10, respectively. The numbers of all three kinds of bursts are roughly equal. The relatively small sample sizes.

Figure 3 shows the distributions of XRFs, XRRs, and GRBs in the $[S_x(2-30 \text{ keV}), S_x(30-400 \text{ keV})]$ plane. As was evident in Figure 2, the three GRB classes seem to form a single distribution. There is a strong, tight positive correlation between

3. X-RAY AND γ -RAY FLUENCES

When the WXM photon time- and energy-tagged (TAG) data are available, we apply a “cut” to the WXM data using only the same manner as we did for GRB 020531 (D. Q. Lamb et al. 2005a, in preparation). We used the spectral survey data (PHA data for WXM, and SP data for FREGATE) when TAG data were not available. The WXM and FREGATE detector response matrix has been well calibrated using observations of the Crab Nebula (WXM, Shiharsaki et al. 2003; FREGATE, Olivie et al. 2003). We use the XSPEC version 11.2.0 software package to do the spectral fits. Details of instruments are given in Kawai et al. (2003) and Shiharsaki et al. (2003) for the WXM, and in Atteia et al. (2003) for the FREGATE.

The time histories of the bursts, details of the spectral-fitting procedure, and time-resolved spectroscopy of some of the bursts are given in a companion paper (T. Sakamoto et al. 2005, in preparation; see also D. Q. Lamb et al. 2005a, in preparation). Other information about the bursts, including sky maps of the HEETE-2 WXM and soft X-ray camera (SXC) localizations, the FREGATE T_{90} and soft X-ray durations of the bursts; whether a host galaxy has been identified; and the redshift of the burst can be found in the First HEETE-2 Burst Catalog (R. Vandenbergk et al. 2005, in preparation).

Table 1 gives some information about the localization and the WXM time histories of the 45 bursts in the sample. Table 2 gives the χ^2 and number of degrees of freedom for all of the spectral fits that we have done. Table 3 gives the details of the spectral class of the bursts (e.g., XRF, XRR, GRB) and the spectral parameters of the best-fit spectral model. Table 4 gives the photon number and energy fluence of each burst in the -30, 30, 400, and 400 keV energy bands, and also energy fluence ratios between 2-30 and 30-400 keV. Table 5 gives the photon number peak flux (1 s) of each burst in 2-30, 30-400, 2-400, and 50-300 keV (BATSE [Burst and Transient Source Experiment] channels 3 and 4; Paciesas et al. 1999) bands.

(2) a power-law times exponential (PLE) model whose three parameters are the power-law index α , the cutoff energy E_0 , and K_{15} ; and (3) the Band function (Band et al. 1993), whose four parameters are the power-law index α , the cutoff energy E_0 , and K_{15} ; and (4) the high-energy power-law index β , the cutoff energy E_0 , and K_{15} . We determine whether the data require a more complicated model (e.g., the PLE model instead of the PL model, or the Band function instead of the PLE model) using the maximum likelihood ratio test, and whether the data require a significance $Q < 10^{-2}$ in order to adopt the more complicated model.

In this study, we consider three spectral models: (1) a power-law model whose two parameters are the power-law index α and the flux cutoff ν_c ; (2) a broken power law model; and (3) a cut-off γ -ray model. The first two models are commonly used to describe the spectra of blazars, while the third model is often used to describe the spectra of AGNs.

Figure 1 illustrates this important point. It shows the threshold bursts as a function of E_{peak} (2–10,000 keV) for *HETE-2* WXM and *FREGATE* old-s in F_x (2–10,000 keV), and the locations of the *HETE-2* bursts discussed in this paper. The figure shows that the threshold for WXM as well as for *FREGATE* are relatively independent of energy, although the energy band for WXM is 2–25 keV. In particular, the threshold for WXM only increases from ~ 1 photon $\text{cm}^{-2} \text{s}^{-1}$ to ~ 2 photons $\text{cm}^{-2} \text{s}^{-1}$ in the 2–10,000 keV energy band as F_{peak} increases from 1 to 500 keV for a typical burst spectrum with $\alpha = -1$ and $\beta = -2.25$. (The corresponding thresholds in the 2–400 keV energy band are ~ 2 photons $\text{cm}^{-2} \text{s}^{-1}$ and ~ 4 photons $\text{cm}^{-2} \text{s}^{-1}$). The figure also shows that (1) the bursts discussed in this paper form a roughly diagonal distribution that extends down to the threshold of WXM, and (2) the F_x (2–10,000 keV) values of the bursts that are GRBs generally lie well above the threshold of WXM. This is strong evidence that the *HETE-2* WXM is not missing many GRBs relative to XRFs and XRRs because of any observational selection effects related to the different spectral shapes of the three kinds of bursts.

is typically in the range of -2 to -3.5 for the photon number spectrum of the bursts (which is the spectrum that matters to detecting the bursts but is not spectral filtering). Hence, the spectra of bursts for which the value of E_0 (and therefore of E_{peak}) is large have large numbers of photons in the X-ray energy range and are easily detected and localized by an X-ray instrument such as WXM, if they are comparable in brightness and in their time histories to bursts with small values of E_0 (and therefore of E_{peak}). Conversely, the detection threshold in peak photon flux F_A for detecting and localizing bursts is relatively independent of the value of E_0 (and therefore of E_{peak}); i.e., it is relatively independent of whether the burst is an XRF, XRR, or GBR.

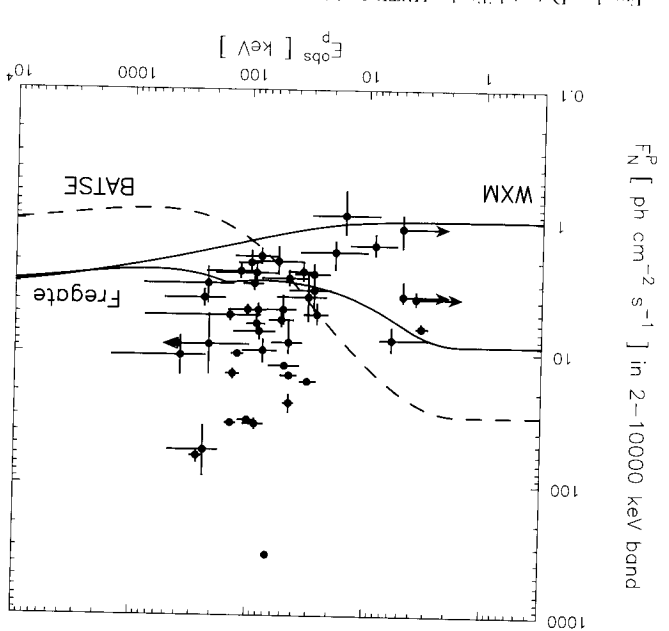


TABLE I
SOME PROPERTIES OF 45 HETE-2 GRBS

GRB	Burst ID	θ_X	θ_Y	TF ^a	TS ^b (s)	EB ^c	R.A.	Decl.	<i>l</i> (deg)	<i>b</i> (deg)	Error ^d (arcmin)	T_{50} (WXM)	T_{90} (WXM)
GRB 010213.....	10805	-2.4	13.6	10 31 36	+05 30 39	239.6	50.3	30.2	8.6 ± 1.2	24.5 ± 1.2	
GRB 010225 ^e	1491	-23.1	1.0	G	1.3	5 120	6.2 ± 1.3	15.9 ± 3.9	
GRB 010326B.....	1496	8.0	15.0	G	.160	5 120	11 24 24	11 09 57	271.2	46.3	36	1.7 ± 0.2	5.2 ± 0.2
GRB 010612.....	1546	13.8	1.2	G	.160	30-400	18 03 18	-32 08 01	359.2	-4.9	36	17.4 ± 0.8	28.5 ± 0.2
GRB 010613.....	1547	-30.5	25.2	G	1.3	30 400	17 00 40	+14 16 05	33.9	30.9	36	23.8 ± 1.2	51.8 ± 0.7
GRB 010629B.....	1573	-26.6	8.3	G	1.3	5 120	16 32 38	-18 43 24	358.6	19.5	15	9.3 ± 0.3	16.2 ± 0.2
GRB 010921.....	1761	-24.0	39.5	G	1.3	5 120	23 01 53	+44 16 12	103.1	14.3	20×15^f
GRB 010928.....	1770	-3.0	35.0	G	1.3	30 400	23 28 55	+30 39 11	102.9	-26.7	16.4×11^g	29.5 ± 3.5	59.0 ± 1.8
GRB 011019.....	10823	18.3	17.6	00 42 50	-12 26 58	114.7	75.2	35	12.2 ± 1.3	31.6 ± 1.2	
GRB 011103.....	1829	-0.3	-10.9	XG	5.12	...	03 20 37	17 40 01	166.1	32.4	...	8.6 ± 1.7	19.7 ± 1.2
GRB 011130.....	1864	13.0	22.8	XG	5.12	...	03 05 36	+03 48 36	174.4	45.2	10	23.8 ± 0.6	39.5 ± 0.4
GRB 011212.....	10827	1.6	9.7	05 00 05	+32 07 39	171.8	-6.3	11	33.2 ± 1.2	72.5 ± 2.8	
GRB 020124.....	1896	14.7	-31.6	G	1.3	30 400	09 32 49	11 27 35	244.9	28.3	12	18.6 ± 1.1	50.2 ± 2.3
GRB 020127.....	1902	-7.5	20.8	G	5.12	30 400	08 15 06	+36 44 31	184.7	31.8	8	6.0 ± 0.3	17.6 ± 1.9
GRB 020317.....	1959	17.1	15.2	G	1.3	5 120	10 23 21	+12 44 38	228.1	52.5	18	2.4 ± 0.4	14.7 ± 0.5
GRB 020331.....	1963	6.9	14.3	G	.160	30 400	13 16 34	-17 52 29	311.3	44.6	10	35.7 ± 1.8	78.7 ± 1.8
GRB 020531.....	2042	22.9	11.3	G	.020	30 400	15 14 45	-19 21 35	343.6	32.0	38	1.1 ± 0.2	2.5 ± 0.3
GRB 020625.....	2081	5.6	10.1	G	5.2	30 400	20 44 14	+07 10 12	53.3	21.1	13.8	13.5 ± 1.2	119.2 ± 2.4
GRB 020801.....	2177	4.7	35.4	G	1.3	30 400	21 02 14	-53 46 13	343.9	40.7	13.9	262.9 ± 4.2	348.9 ± 4.4
GRB 020812.....	2257	-15.3	-12.1	G	1.3	30 400	20 38 48	-05 23 34	40.7	-26.3	13.8	14.1 ± 0.6	42.0 ± 1.0
GRB 020813.....	2262	0.0	3.8	G	1.3	30 400	19 46 38	-19 35 16	20.8	-20.7	1(S)	>30.0	>89.0
GRB 020819.....	2275	17.7	22.5	G	.160	30 400	23 27 07	+06 21 50	88.5	-50.8	7	11.5 ± 0.3	46.9 ± 2.0
GRB 020903.....	2314	4.2	12.6	XG	5.12	...	22 49 25	-20 53 59	38.9	61.5	16.7	4.8 ± 0.4	10.0 ± 0.7
GRB 021004.....	2380	3.9	-12.4	G	5.2	30 400	00 26 57	+18 55 44	114.9	-43.6	2(S)	26.6 ± 1.0	77.1 ± 2.6
GRB 021021.....	10623	15.2	11.9	00 17 23	-01 37 00	103.8	-63.2	20	22.1 ± 1.2	56.5 ± 1.2	
GRB 021104.....	2434	22.6	22.9	G	1.3	5 120	03 53 48	+37 57 12	158.1	-12.2	26	10.2 ± 0.5	18.1 ± 0.2
GRB 021112.....	2448	12.2	27.1	G	1.3	5 120	02 36 52	-148 50 56	140.2	-10.5	20	6.8 ± 1.2	14.7 ± 1.1
GRB 021211.....	2493	-12.6	0.0	G	.160	30 400	08 09 00	+06 44 20	215.7	20.3	2(S)	3.1 ± 0.1	13.3 ± 0.3
GRB 030115.....	2533	13.0	3.1	G	1.3	30 400	11 18 30	+15 02 17	237.4	65.2	2(S)	9.2 ± 0.5	49.6 ± 4.3
GRB 030226.....	10893	-13.0	16.3	11 33 01	+25 53 56	212.5	72.4	2(S)	66.4 ± 3.9	137.7 ± 4.9	
GRB 030323.....	2640	4.1	35.1	XG	.320	...	11 06 54	-21 51 00	273.0	34.9	18	13.9 ± 1.6	32.6 ± 2.7
GRB 030324.....	2641	26.4	0.6	G	1.3	30 400	13 37 11	-00 19 22	326.6	60.4	7	8.9 ± 0.3	25.8 ± 0.8
GRB 030328.....	2650	5.1	7.1	G	1.3	5 120	12 10 51	-09 21 05	286.4	52.2	1(S)	106.9 ± 1.2	315.8 ± 3.0
GRB 030329.....	2652	26.7	-29.0	G	1.3	5 120	10 44 49	+21 28 44	217.1	60.7	2(S)	12.1 ± 0.2	33.1 ± 0.5
GRB 030416.....	10897	-2.0	-11.3	11 06 51	-02 52 58	258.8	50.8	7	19.7 ± 1.7	61.5 ± 1.2	
GRB 030418.....	2686	7.5	-9.7	XG	13.280	...	10 54 53	-06 59 22	259.1	45.7	9	38.7 ± 0.9	117.6 ± 0.7
GRB 030429.....	2695	8.9	11.8	XG	6.72	...	12 13 06	-20 56 00	291.0	41.1	1(S)	38.4 ± 1.5	77.4 ± 1.2
GRB 030519.....	2716	41.0	16.2	G	.160	30 400	14 58 18	32 56 57	331.5	22.8	30	6.1 ± 0.6	13.8 ± 0.7
GRB 030528.....	2724	20.7	6.1	G	1.3	30 400	17 04 02	-22 38 59	0.0	11.3	2(S)	20.8 ± 1.2	49.2 ± 1.2
GRB 030723.....	2777	1.6	10.9	XG	6.72	WXM	21 49 30	-27 42 06	21.2	-49.9	2(S)	9.9 ± 0.3	20.2 ± 0.5
GRB 030725.....	2779	18.4	33.1	G	.160	5 120	20 33 47	-50 45 49	348.2	-36.6	14.4	68.3 ± 3.4	200.0 ± 2.5
GRB 030821.....	2814	12.1	32.5	G	1.3	30 400	21 42 33	-45 12 12	354.3	-48.5	120×10	11.7 ± 1.5	22.9 ± 0.5
GRB 030823.....	2818	11.7	-32.7	G	5.2	5 120	21 30 47	+21 59 46	73.2	-21.0	5.4	30.2 ± 1.4	66.4 ± 1.9
GRB 030824.....	2821	-29.8	-31.4	G	1.3	5 120	00 05 02	+19 55 37	108.3	-41.6	11.2	13.1 ± 1.8	36.4 ± 0.4
GRB 030913.....	2849	-2.1	4.6	G	1.3	30-400	20 58 02	-02 12 32	46.5	-29.0	30	2.9 ± 0.3	6.7 ± 0.3

NOTE.—Units of right ascension are hours, minutes, and seconds, and units of declination are degrees, arcminutes, and arcseconds.

^a Triggered type; G: FREGATE triggered, XG: FREGATE triggered by XDSP.

^b Trigger timescale.

^c Trigger energy band in keV.

^d Location error radius (90% confidence). "S" indicates localization by the SXC.

^e Since the attitude control camera was not operational, the celestial coordinates are not available.

^f Error is $20^\circ \times 15'$.

^g Error is $16.4' \times 11'$.

TABLE 2
THE χ^2 AND dof FOR ALL OF THE SPECTRAL FITS THAT WE HAVE DONE

GRB	χ^2/dof	PL _a	PL _b	Band _c	Comment
GRB 010213.....	70.2/45	51.3/45	41.4/44	Fix α for PLF and Band	
GRB 010225.....	43.9/40	36.1/39	36.1/38	Fix α for PLF and Band	
GRB 010326B.....	120.2/112	95.0/111	95.0/110	Fix α for PLF and Band	
GRB 010612.....	66.6/66	57.5/65	56.8/64	Fix α for PLF and Band	
GRB 010613.....	198.8/136	123.2/135	105.2/134	Fix α for PLF and Band	
GRB 010921.....	173.9/141	131.5/140	131.1/139	Fix α for PLF and Band	
GRB 010928.....	159.9/126	103.1/125	102.7/124	Fix α for PLF and Band	
GRB 011110.....	40.7/40	38.7/39	40.7/38	Fix α for PLF and Band	
GRB 011103.....	48.1/38	45.0/37	44.0/36	Fix α for PLF and Band	
GRB 011109.....	61.8/68	58.1/68	58.1/67	Fix α for PLF and Band	
GRB 011130.....	42.8/52	42.9/53	42.9/54	Fix α for PLF and Band	
GRB 011122.....	106.4/111	82.1/110	82.5/109	Fix α for PLF and Band	
GRB 020127.....	106.4/111	81.3/111	81.2/110	Fix α for PLF and Band	
GRB 020317.....	65.7/54	48.9/53	48.9/52	Fix α for PLF and Band	
GRB 020331.....	140.2/112	81.2/112	81.2/111	Fix α for PLF and Band	
GRB 020531.....	144.7/142	117.2/141	117.0/140	Fix α for PLF and Band	
GRB 020625.....	46.5/55	43.0/54	43.0/54	Fix α for PLF and Band	
GRB 020801.....	157.3/142	103.0/141	89.3/140	Fix α for PLF and Band	
GRB 020812.....	53.3/69	45.2/68	45.2/67	Fix α for PLF and Band	
GRB 020813.....	100.7/842	27.3/841	16.2/840	Fix α for PLF and Band	
GRB 020819.....	209.9/110	109.0/109	102.1/108	Fix α for PLF and Band	
GRB 021112.....	83.6/62	68.7/61	68.7/60	Fix α for PLF and Band	
GRB 021115.....	68.8/68	54.4/67	54.4/66	Fix α for PLF and Band	
GRB 021211.....	583.7/142	172.3/141	160.9/140	Fix α for PLF and Band	
GRB 030226.....	172.1/140	124.2/139	124.2/138	Fix α for PLF and Band	
GRB 030323.....	27.6/33	27.6/32	27.6/31	Fix α for PLF and Band	
GRB 030324.....	71.2/77	67.1/76	67.1/75	Fix α for PLF and Band	
GRB 030328.....	44.4/142	142.0/141	137.5/140	Fix α for PLF and Band	
GRB 030416.....	47.0/54	53.4/53	47.0/52	Fix α for PLF and Band	
GRB 030418.....	76.2/69	63.1/68	63.1/67	Fix α for PLF and Band	
GRB 030429.....	76.4/69	48.9/68	48.9/67	Fix α for PLF and Band	
GRB 030519.....	785.5/126	151.2/125	92.0/124	Fix α for PLF and Band	
GRB 030821.....	177.1/99	95.1/98	95.0/97	Fix α for PLF and Band	
GRB 030823.....	113.1/111	77.3/110	77.3/109	Fix α for PLF and Band	
GRB 030824.....	43.1/53	42.3/52	42.1/51	Fix α for PLF and Band	
GRB 030913.....	49.4/54	39.2/53	38.6/52	Fix α for PLF and Band	

^a Band; Band function.

^b PLF; power-law times exponential cutoff.

^c PL; power-law.

Note.—The value pairs denoted with an asterisk are for the spectral model that we have chosen as characterizing the spectrum of the burst.

TABLE 3
SPECTRAL PARAMETERS OF 45 HETE-2 GRBS

GRB	Class ^a	Model ^b	α	β	E_{peak} (keV)	K_{15}^{c} (10^{-2} photons cm $^{-2}$ s $^{-1}$ keV $^{-1}$)	χ^2	dof
GRB 010213.....	XRF	Band	-1.0 (fixed)	-3.0 $^{+0.2}_{-0.5}$	3.4 \pm 0.4	45 $^{+8}_{-5}$	41.4	44
GRB 010225.....	XRF	PLE	1.3 \pm 0.3	...	32 $^{+27}_{-9}$	7 $^{+3}_{-2}$	36.1	39
GRB 010326B†.....	XRR	PLE	-1.1 $^{+0.3}_{-0.2}$...	52 $^{+19}_{-11}$	13 $^{+3}_{-3}$	95.0	111
GRB 010612.....	GRB	PLE	1.1 \pm 0.2	...	240 $^{+290}_{-82}$	2.9 \pm 0.4	57.5	65
GRB 010613.....	XRR	Band	-1.0 \pm 0.3	2.0 $^{+0.1}_{-0.2}$	46 $^{+18}_{-10}$	15 $^{+4}_{-2}$	105.2	134
GRB 010629B.....	XRR	PLE	1.1 \pm 0.1	...	46 $^{+5}_{-4}$	20 \pm 2	89.9	110
GRB 010921†.....	XRR	PLE	1.6 \pm 0.1	...	89 $^{+22}_{-14}$	42 \pm 2	131.5	140
GRB 010928†.....	GRB	PLE	-0.7 \pm 0.1	...	410 $^{+120}_{-75}$	6.3 \pm 0.6	103.1	125
GRB 011019.....	XRF	PLE	-1.4 (fixed)	...	19 $^{+18}_{-9}$	2.5 $^{+0.8}_{-0.6}$	58.1	68
GRB 011103†.....	XRR	PL	1.7 $^{+0.2}_{-0.3}$	2.7 \pm 0.9	48.1	38
GRB 011130.....	XRF	PL	...	-2.7 \pm 0.3	<3.9 ^d	0.7 \pm 0.3	40.7	40
GRB 011212.....	XRF	PL	...	2.1 \pm 0.2	...	0.7 \pm 0.2	42.9	54
GRB 020124.....	XRR	PLE	-0.8 $^{+0.2}_{-0.1}$...	87 $^{+18}_{-13}$	9 \pm 1	67.5	95
GRB 020127.....	XRR	PLE	-1.0 \pm 0.1	...	100 $^{+47}_{-24}$	4.5 $^{+0.6}_{-0.5}$	82.1	110
GRB 020317.....	XRF	PLE	-0.6 $^{+0.6}_{-0.5}$...	28 $^{+13}_{-7}$	7 $^{+8}_{-3}$	48.9	53
GRB 020331.....	GRB	PLE	0.8 \pm 0.1	...	92 $^{+21}_{-14}$	4.0 $^{+0.5}_{-0.4}$	81.3	111
GRB 020531.....	GRB	PLE	-0.8 \pm 0.1	...	230 $^{+110}_{-58}$	21 \pm 2	117.2	141
GRB 020625.....	XRF	PLE	-1.1 (fixed)	...	8.5 $^{+3.1}_{-2.9}$	2.8 $^{+1.1}_{-0.8}$	43.0	55
GRB 020801†.....	GRB	Band	0.3 $^{+0.4}_{-0.3}$	2.0 $^{+0.2}_{-0.3}$	53 $^{+14}_{-11}$	6 $^{+2}_{-1}$	89.3	140
GRB 020812.....	XRR	PLE	-1.1 \pm 0.3	...	88 $^{+110}_{-30}$	2.3 $^{+0.6}_{-0.5}$	45.2	68
GRB 020813†.....	GRB	Band	-0.94 $^{+0.03}_{-0.03}$	-1.57 $^{+0.03}_{-0.04}$	140 $^{+14}_{-13}$	20.7 \pm 0.5	162.4	140
GRB 020819.....	XRR	Band	-0.9 $^{+0.2}_{-0.1}$	-2.0 $^{+0.2}_{-0.5}$	50 $^{+18}_{-12}$	11 $^{+3}_{-2}$	102.1	108
GRB 020903.....	XRF	PL	...	2.6 $^{+0.4}_{-0.6}$	<5.0(2.6 $^{+1.4}_{-0.8}$) ^d	0.4 \pm 0.3	22.0	26
GRB 021004.....	XRR	PLE	1.0 \pm 0.2	...	80 $^{+53}_{-23}$	2.8 $^{+0.6}_{-0.5}$	64.5	68
GRB 021021.....	XRF	PLE	-1.3 (fixed)	...	15 $^{+14}_{-8}$	1.2 $^{+0.5}_{-0.4}$	36.0	41
GRB 021104†.....	XRF	PLE	-1.1 \pm 0.5	...	28 $^{+17}_{-8}$	8 $^{+5}_{-3}$	28.3	38
GRB 021112.....	XRR	PLE	-0.9 $^{+0.4}_{-0.3}$...	57 $^{+39}_{-21}$	7 $^{+4}_{-2}$	68.7	61
GRB 021211.....	XRR	Band	-0.9 \pm 0.1	-2.2 $^{+0.1}_{-0.3}$	46 $^{+8}_{-6}$	33 $^{+4}_{-3}$	160.9	140
GRB 030115.....	XRR	PLE	-1.3 \pm 0.1	...	83 $^{+53}_{-22}$	3.5 \pm 0.5	54.4	67
GRB 030226.....	GRB	PLE	-0.9 \pm 0.2	...	97 $^{+27}_{-17}$	3.5 \pm 0.4	124.2	139
GRB 030323.....	XRR	PL	-1.6 $^{+0.2}_{-0.3}$	2.2 $^{+0.6}_{-0.7}$	27.6	33
GRB 030324.....	XRR	PLE	1.5 \pm 0.1	...	150 $^{+630}_{-65}$	4.9 $^{+0.7}_{-0.6}$	67.1	76
GRB 030328.....	GRB	Band	1.14 $^{+0.03}_{-0.03}$	2.1 $^{+0.2}_{-0.4}$	130 $^{+14}_{-13}$	6.6 \pm 0.2	137.5	140
GRB 030329.....	XRR	Band	-1.26 $^{+0.01}_{-0.02}$	-2.28 $^{+0.05}_{-0.06}$	68 \pm 2	146 \pm 2	213.7	139
GRB 030416.....	XRF	PL	...	-2.3 $^{+0.1}_{-0.2}$	<3.8(2.6 $^{+0.5}_{-1.8}$) ^d	0.9 \pm 0.2	47.0	54
GRB 030418.....	XRR	PLE	-1.5 \pm 0.1	...	46 $^{+32}_{-14}$	2.4 $^{+0.5}_{-0.4}$	63.2	68
GRB 030429.....	XRF	PLE	-1.1 $^{+0.3}_{-0.2}$...	35 $^{+12}_{-8}$	4.1 $^{+1.3}_{-0.9}$	49.0	68
GRB 030519†.....	GRB	Band	-0.8 \pm 0.1	1.7 \pm 0.1	138 $^{+18}_{-15}$	73 \pm 2	92.0	124
GRB 030528†.....	XRF	Band	-1.3 $^{+0.2}_{-0.1}$	2.7 $^{+0.3}_{-1.0}$	32 \pm 5	14 \pm 2	88.2	109
GRB 030723.....	XRF	PL	...	-1.9 \pm 0.2	<8.9 ^d	1.0 \pm 0.2	135.2	142
GRB 030725.....	XRR	PLE	1.51 $^{+0.04}_{-0.04}$...	102 $^{+19}_{-14}$	15.7 \pm 0.5	150.7	141
GRB 030821.....	XRR	PLE	0.9 \pm 0.1	...	84 $^{+15}_{-11}$	8.7 $^{+0.8}_{-0.7}$	95.1	98
GRB 030823.....	XRF	PLE	1.3 \pm 0.2	...	27 $^{+8}_{-5}$	8 \pm 2	77.9	110
GRB 030824.....	XRF	PL	...	2.1 \pm 0.1	<8.7(6.1 $^{+1.9}_{-4.2}$) ^d	5.3 \pm 0.8	43.1	53
GRB 030913.....	GRB	PLE	-0.8 $^{+0.3}_{-0.2}$...	120 $^{+110}_{-37}$	3.5 $^{+0.8}_{-0.7}$	39.2	53

NOTE.—Daggers denote that the constant factor is multiplied by the spectral model.

^a GRB classification—XRF: X-ray-flash; XRR: X-ray-rich GRB; GRB: GRB.

^b Spectral model—PL: power-law; PLE: power-law times exponential cutoff; Band: Band function.

^c Normalization at 15 keV.

^d 99.7% upper limit and 90% confidence interval (in parentheses) derived by the *constrained* Band function.

GRB	DETECTION (s)	2-30 keV	30-400 keV	2-400 keV	2-400 keV	X-Ray/L-Ray Ratio
		Photon Filter (photons cm ⁻²)	Energy Filter (10 ⁻⁷ ergs cm ⁻²)			
PHOTON NUMBER AND PHOTON ENERGY FILTERS OF 45 HETE-2 GRBS						
TABLE 4						
GRB 010213.....	344	111 ± 5	0.7 ± 0.3	112 ± 5	7.9 ± 0.3	0.7 ± 0.3
GRB 010225.....	9.8	28 ± 4	2.7 ± 1.0	31 ± 4	3.5 ± 0.4	2.4 ± 0.3
GRB 010326B.....	3.5	17 ± 3	3.2 ± 0.6	20 ± 3	2.4 ± 0.3	6 ± 1
GRB 010612.....	47.2	57 ± 13	29 ± 2	86 ± 14	8.8 ± 1.3	50 ± 7
GRB 010613.....	141.6	672 ± 110	169 ± 6	840 ± 10	102 ± 7	32 ± 14
GRB 010629B.....	24.6	183 ± 20	30 ± 2	234 ± 20	28.6 ± 2.3	54.0 ± 3.3
GRB 010928.....	23.9	610 ± 49	89 ± 4	699 ± 48	72 ± 3	113 ± 8
GRB 010927.....	23.9	610 ± 49	89 ± 4	699 ± 48	72 ± 3	113 ± 8
GRB 011109.....	14.8	28 ± 6	1.5 ± 1	29 ± 6	3.0 ± 0.6	1.1 ± 1
GRB 011130.....	34.6	71 ± 10	105 ± 10	175 ± 10	226 ± 10	239 ± 9
GRB 011212.....	57.7	47 ± 7	2.3 ± 1.7	50 ± 8	4.2 ± 0.6	3.4 ± 1.7
GRB 020124.....	40.6	115 ± 12	51 ± 5	196 ± 13	19.7 ± 1.4	61 ± 8
GRB 0202531.....	1.0	7.5 ± 1.1	1.3 ± 0.5	13.7 ± 1.2	1.3 ± 0.1	11.1 ± 1.4
GRB 020625.....	41.9	25 ± 4	0.2 ± 0.3	25 ± 4	2.4 ± 0.6	0.1 ± 0.4
GRB 020801.....	118.0	131 ± 27	70 ± 5	201 ± 23	26 ± 3	95 ± 11
GRB 020812.....	60.2	53 ± 10	16 ± 3	69 ± 11	8 ± 1	19 ± 8
GRB 020813.....	113.0	845 ± 23	480 ± 5	1325 ± 22	139 ± 3	979 ± 13
GRB 020819.....	50.2	163 ± 9	46 ± 4	209 ± 10	2.4 ± 0.3	46 ± 4
GRB 020903.....	13.0	13 ± 3	0.2 ± 0.1	25.2 ± 1.1	0.8 ± 0.2	46 ± 4
GRB 021115.....	36.0	59 ± 5	12.6 ± 1.8	71 ± 6	7.9 ± 0.6	15.5 ± 2.3
GRB 021116.....	78.6	114 ± 10	3.2 ± 0.8	117 ± 10	9.0 ± 0.9	1076 ± 11
GRB 0212029.....	62.9	4120 ± 42	843 ± 6	751 ± 12	82 ± 1	287 ± 14
GRB 021228.....	199.2	556 ± 12	9.0 ± 1.3	53 ± 5	5.5 ± 0.4	13 ± 2
GRB 02124.....	15.7	44 ± 4	5.5 ± 1.8	3.4 ± 1.3	9 ± 1.4	12 ± 4
GRB 02126.....	19.6	29 ± 16	3.3 ± 3	114 ± 10	13 ± 1	43 ± 6
GRB 02127.....	49.2	50 ± 5	1.5 ± 3	15 ± 6	7.7 ± 0.7	18.5 ± 8
GRB 02129.....	49.7	50 ± 5	0.2 ± 0.1	13 ± 3	0.8 ± 0.2	46 ± 4
GRB 02130.....	13.0	13 ± 2	0.2 ± 0.1	11 ± 2	1.3 ± 0.3	2.1 ± 0.9
GRB 02140.....	4.0	9 ± 2	2.1 ± 0.6	11 ± 2	2.1 ± 1.1	3.5 ± 0.9
GRB 02142.....	31.4	79 ± 21	7.5 ± 2.3	9.6 ± 2.1	16 ± 3	17 ± 7
GRB 02144.....	49.2	23 ± 4	0.9 ± 0.1	24 ± 3	2.5 ± 0.6	0.6 ± 0.1
GRB 02146.....	49.7	50 ± 5	1.5 ± 3	65 ± 6	18.5 ± 8	26.5 ± 7
GRB 02147.....	49.7	50 ± 5	0.2 ± 0.1	13 ± 3	0.8 ± 0.2	46 ± 4
GRB 02149.....	8.0	74.6 ± 2.4	18.9 ± 0.9	93.4 ± 2.6	23.7 ± 2.0	35.3 ± 2.1
GRB 02151.....	13.0	13 ± 3	0.2 ± 0.1	11 ± 2	1.3 ± 0.3	2.1 ± 0.9
GRB 02152.....	4.0	9 ± 2	2.1 ± 0.6	11 ± 2	2.1 ± 1.1	3.5 ± 0.9
GRB 02154.....	31.4	79 ± 21	7.5 ± 2.3	9.6 ± 2.1	16 ± 3	17 ± 7
GRB 02156.....	49.2	23 ± 4	0.9 ± 0.1	24 ± 3	2.5 ± 0.6	0.6 ± 0.1
GRB 02157.....	15.7	44 ± 4	5.5 ± 1.8	3.4 ± 1.3	9 ± 1.4	12 ± 4
GRB 02158.....	19.6	29 ± 16	3.3 ± 3	114 ± 10	13 ± 1	43 ± 6
GRB 02159.....	36.0	59 ± 5	12.6 ± 1.8	71 ± 6	7.9 ± 0.6	15.5 ± 2.3
GRB 02160.....	110.1	143 ± 9	17 ± 4	161 ± 10	9.0 ± 0.9	1076 ± 11
GRB 02161.....	78.6	114 ± 10	3.2 ± 0.8	117 ± 10	9.0 ± 0.9	1076 ± 11
GRB 02162.....	62.9	4120 ± 42	843 ± 6	751 ± 12	82 ± 1	287 ± 14
GRB 02163.....	199.2	556 ± 12	9.0 ± 1.3	53 ± 5	5.5 ± 0.4	13 ± 2
GRB 02164.....	15.7	44 ± 4	5.5 ± 1.8	3.4 ± 1.3	9 ± 1.4	12 ± 4
GRB 02165.....	19.6	29 ± 16	3.3 ± 3	114 ± 10	13 ± 1	43 ± 6
GRB 02166.....	36.0	59 ± 5	12.6 ± 1.8	71 ± 6	7.9 ± 0.6	15.5 ± 2.3
GRB 02167.....	110.1	143 ± 9	17 ± 4	161 ± 10	9.0 ± 0.9	1076 ± 11
GRB 02168.....	78.6	114 ± 10	3.2 ± 0.8	117 ± 10	9.0 ± 0.9	1076 ± 11
GRB 02169.....	62.9	4120 ± 42	843 ± 6	751 ± 12	82 ± 1	287 ± 14
GRB 02170.....	199.2	556 ± 12	9.0 ± 1.3	53 ± 5	5.5 ± 0.4	13 ± 2
GRB 02171.....	15.7	44 ± 4	5.5 ± 1.8	3.4 ± 1.3	9 ± 1.4	12 ± 4
GRB 02172.....	19.6	29 ± 16	3.3 ± 3	114 ± 10	13 ± 1	43 ± 6
GRB 02173.....	36.0	59 ± 5	12.6 ± 1.8	71 ± 6	7.9 ± 0.6	15.5 ± 2.3
GRB 02174.....	110.1	143 ± 9	17 ± 4	161 ± 10	9.0 ± 0.9	1076 ± 11
GRB 02175.....	78.6	114 ± 10	3.2 ± 0.8	117 ± 10	9.0 ± 0.9	1076 ± 11
GRB 02176.....	62.9	4120 ± 42	843 ± 6	751 ± 12	82 ± 1	287 ± 14
GRB 02177.....	199.2	556 ± 12	9.0 ± 1.3	53 ± 5	5.5 ± 0.4	13 ± 2
GRB 02178.....	15.7	44 ± 4	5.5 ± 1.8	3.4 ± 1.3	9 ± 1.4	12 ± 4
GRB 02179.....	19.6	29 ± 16	3.3 ± 3	114 ± 10	13 ± 1	43 ± 6
GRB 02180.....	36.0	59 ± 5	12.6 ± 1.8	71 ± 6	7.9 ± 0.6	15.5 ± 2.3
GRB 02181.....	110.1	143 ± 9	17 ± 4	161 ± 10	9.0 ± 0.9	1076 ± 11
GRB 02182.....	78.6	114 ± 10	3.2 ± 0.8	117 ± 10	9.0 ± 0.9	1076 ± 11
GRB 02183.....	62.9	4120 ± 42	843 ± 6	751 ± 12	82 ± 1	287 ± 14
GRB 02184.....	199.2	556 ± 12	9.0 ± 1.3	53 ± 5	5.5 ± 0.4	13 ± 2
GRB 02185.....	15.7	44 ± 4	5.5 ± 1.8	3.4 ± 1.3	9 ± 1.4	12 ± 4
GRB 02186.....	19.6	29 ± 16	3.3 ± 3	114 ± 10	13 ± 1	43 ± 6
GRB 02187.....	36.0	59 ± 5	12.6 ± 1.8	71 ± 6	7.9 ± 0.6	15.5 ± 2.3
GRB 02188.....	110.1	143 ± 9	17 ± 4	161 ± 10	9.0 ± 0.9	1076 ± 11
GRB 02189.....	78.6	114 ± 10	3.2 ± 0.8	117 ± 10	9.0 ± 0.9	1076 ± 11
GRB 02190.....	62.9	4120 ± 42	843 ± 6	751 ± 12	82 ± 1	287 ± 14
GRB 02191.....	199.2	556 ± 12	9.0 ± 1.3	53 ± 5	5.5 ± 0.4	13 ± 2
GRB 02192.....	15.7	44 ± 4	5.5 ± 1.8	3.4 ± 1.3	9 ± 1.4	12 ± 4
GRB 02193.....	19.6	29 ± 16	3.3 ± 3	114 ± 10	13 ± 1	43 ± 6
GRB 02194.....	36.0	59 ± 5	12.6 ± 1.8	71 ± 6	7.9 ± 0.6	15.5 ± 2.3
GRB 02195.....	110.1	143 ± 9	17 ± 4	161 ± 10	9.0 ± 0.9	1076 ± 11
GRB 02196.....	78.6	114 ± 10	3.2 ± 0.8	117 ± 10	9.0 ± 0.9	1076 ± 11
GRB 02197.....	62.9	4120 ± 42	843 ± 6	751 ± 12	82 ± 1	287 ± 14
GRB 02198.....	199.2	556 ± 12	9.0 ± 1.3	53 ± 5	5.5 ± 0.4	13 ± 2
GRB 02199.....	15.7	44 ± 4	5.5 ± 1.8	3.4 ± 1.3	9 ± 1.4	12 ± 4
GRB 02200.....	19.6	29 ± 16	3.3 ± 3	114 ± 10	13 ± 1	43 ± 6
GRB 02201.....	36.0	59 ± 5	12.6 ± 1.8	71 ± 6	7.9 ± 0.6	15.5 ± 2.3
GRB 02202.....	110.1	143 ± 9	17 ± 4	161 ± 10	9.0 ± 0.9	1076 ± 11
GRB 02203.....	78.6	114 ± 10	3.2 ± 0.8	117 ± 10	9.0 ± 0.9	1076 ± 11
GRB 02204.....	62.9	4120 ± 42	843 ± 6	751 ± 12	82 ± 1	287 ± 14
GRB 02205.....	199.2	556 ± 12	9.0 ± 1.3	53 ± 5	5.5 ± 0.4	13 ± 2
GRB 02206.....	15.7	44 ± 4	5.5 ± 1.8	3.4 ± 1.3	9 ± 1.4	12 ± 4
GRB 02207.....	19.6	29 ± 16	3.3 ± 3	114 ± 10	13 ± 1	43 ± 6
GRB 02208.....	36.0	59 ± 5	12.6 ± 1.8	71 ± 6	7.9 ± 0.6	15.5 ± 2.3
GRB 02209.....	110.1	143 ± 9	17 ± 4	161 ± 10	9.0 ± 0.9	1076 ± 11
GRB 02210.....	78.6	114 ± 10	3.2 ± 0.8	117 ± 10	9.0 ± 0.9	1076 ± 11
GRB 02211.....	62.9	4120 ± 42	843 ± 6	751 ± 12	82 ± 1	287 ± 14
GRB 02212.....	199.2	556 ± 12	9.0 ± 1.3	53 ± 5	5.5 ± 0.4	13 ± 2
GRB 02213.....	15.7	44 ± 4	5.5 ± 1.8	3.4 ± 1.3	9 ± 1.4	12 ± 4
GRB 02214.....	19.6	29 ± 16	3.3 ± 3	114 ± 10	13 ± 1	43 ± 6
GRB 02215.....	36.0	59 ± 5	12.6 ± 1.8	71 ± 6	7.9 ± 0.6	15.5 ± 2.3
GRB 02216.....	110.1	143 ± 9	17 ± 4	161 ± 10	9.0 ± 0.9	1076 ± 11
GRB 02217.....	78.6	114 ± 10	3.2 ± 0.8	117 ± 10	9.0 ± 0.9	1076 ± 11
GRB 02218.....	62.9	4120 ± 42	843 ± 6	751 ± 12	82 ± 1	287 ± 14
GRB 02219.....	199.2	556 ± 12	9.0 ± 1.3	53 ± 5	5.5 ± 0.4	13 ± 2
GRB 02220.....	15.7	44 ± 4	5.5 ± 1.8	3.4 ± 1.3	9 ± 1.4	12 ± 4
GRB 02221.....	19.6	29 ± 16	3.3 ± 3	114 ± 10	13 ± 1	43 ± 6
GRB 02222.....	36.0	59 ± 5	12.6 ± 1.8	71 ± 6	7.9 ± 0.6	15.5 ± 2.3
GRB 02223.....	110.1	143 ± 9	17 ± 4	161 ± 10	9.0 ± 0.9	1076 ± 11
GRB 02224.....	78.6	114 ± 10	3.2 ± 0.8	117 ± 10	9.0 ± 0.9	1076 ± 11
GRB 02225.....	62.9	4120 ± 42	843 ± 6	751 ± 12	82 ± 1	287 ± 14
GRB 02226.....	199.2	556 ± 12	9.0 ± 1.3	53 ± 5	5.5 ± 0.4	13 ± 2
GRB 02227.....	15.7	44 ± 4	5.5 ± 1.8	3.4 ± 1.3	9 ± 1.4	12 ± 4
GRB 02228.....	19.6	29 ± 16	3.3 ± 3	114 ± 10	13 ± 1	43 ± 6
GRB 02229.....	36.0	59 ± 5	12.6 ± 1.8	71 ± 6	7.9 ± 0.6	15.5 ± 2.3
GRB 02230.....	110.1	143 ± 9	17 ± 4	161 ± 10	9.0 ± 0.9	1076 ± 11
GRB 02231.....	78.6	114 ± 10	3.2 ± 0.8	117 ± 10	9.0 ± 0.9	1076 ± 11
GRB 02232.....	62.9	4120 ± 42	843 ± 6	751 ± 12	82 ± 1	287 ± 14
GRB 02233.....	199.2	556 ± 12	9.0 ± 1.3	53 ± 5	5.5 ± 0.4	13 ± 2
GRB 02234.....	15.7	44 ± 4	5.5 ± 1.8	3.4 ± 1.3	9 ± 1.4	12 ± 4
GRB 02235.....	19.6	29 ± 16	3.3 ± 3	114 ± 10	13 ± 1	43 ± 6
GRB 02236.....	36.0	59 ± 5	12.6 ± 1.8	71 ± 6	7.9 ± 0.6	15.5 ± 2.3
GRB 02237.....	110.1	143 ± 9	17 ± 4	161 ± 10	9.0 ± 0.9	1076 ± 11
GRB 02238.....	78.6	114 ± 10	3.2 ± 0.8	117 ± 10	9.0 ± 0.9	1076 ± 11
GRB 02239.....	62.9	4120 ± 42	843 ± 6	751 ± 12	82 ± 1	287 ± 14
GRB 02240.....	199.2	556 ± 12	9.0 ± 1.3	53 ± 5	5.5 ± 0.4	13 ± 2
GRB 02241.....	15.7	44 ± 4	5.5 ± 1.8	3.4 ± 1.3	9 ± 1.4	12 ± 4
GRB 02242.....	19.6	29 ± 16	3.3 ± 3	114 ± 10	13 ± 1	43 ± 6
GRB 02243.....	36.0	59 ± 5	12			

TABLE 5
PEAK (1 s) PHOTON NUMBER FLUX OF 45 *HETE*-2 GRBS

GRB	Class ^a	Model ^b	$F_{\text{peak}(2-30 \text{ keV})}^N$ (photons cm $^{-2}$ s $^{-1}$)	$F_{\text{peak}(30-400 \text{ keV})}^N$	$F_{\text{peak}(2-400 \text{ keV})}^N$	$F_{\text{peak}(50-300 \text{ keV})}^N$
GRB 010213.....	XRF	Band	6.3 ± 0.8	$(3.0 \pm 0.6) \times 10^{-3}$	6.3 ± 0.8	$(1.1 \pm 0.2) \times 10^{-2}$
GRB 010225.....	XRF	PLE	5.1 ± 2.4	0.3 ± 0.2	5.5 ± 2.4	$(9.6 \pm 9.4) \times 10^{-2}$
GRB 010326B.....	XRR	PLE	11 ± 3	1.5 ± 0.4	12 ± 3	0.7 ± 0.2
GRB 010612.....	GRB	PLE	4.3 ± 1.2	4.4 ± 0.5	8.7 ± 1.4	3.1 ± 0.4
GRB 010613.....	XRR	Band	25 ± 12	2.7 ± 0.9	27 ± 11	1.2 ± 0.4
GRB 010629B.....	XRR	PLE	39 ± 7	4.2 ± 0.4	43 ± 7	1.9 ± 0.3
GRB 010921.....	XRR	PLE	34 ± 4	5.7 ± 0.5	40 ± 4	3.2 ± 0.3
GRB 010928.....	GRB	PLE	3.8 ± 0.8	6.9 ± 0.5	11 ± 1	5.0 ± 0.5
GRB 011019.....	XRF	PL	3.6 ± 1.4	0.2 ± 0.1	3.8 ± 1.4	$(7.4 \pm 7.3) \times 10^{-2}$
GRB 011103.....	XRR	PL	4.4 ± 1.1	0.1 ± 0.1	4.6 ± 1.1	$(6.5 \pm 4.3) \times 10^{-2}$
GRB 011130.....	XRF	PL	5.3 ± 1.3	$(8.2 \pm 6.3) \times 10^{-2}$	5.4 ± 1.3	$(3.6 \pm 3.2) \times 10^{-2}$
GRB 011212.....	XRF	PL	1.1 ± 1.0	$<7.7 \times 10^{-2}$	1.1 ± 1.0	$<4.4 \times 10^{-2}$
GRB 020124.....	XRR	PLE	6.9 ± 1.6	2.5 ± 0.4	9.4 ± 1.8	1.4 ± 0.3
GRB 020127.....	XRR	PLE	6.0 ± 1.2	2.2 ± 0.4	8.1 ± 1.5	1.3 ± 0.3
GRB 020317.....	XRF	PLE	4.6 ± 1.0	0.6 ± 0.3	5.3 ± 1.1	0.2 ± 0.1
GRB 020331.....	GRB	PLE	1.9 ± 0.4	1.7 ± 0.2	3.7 ± 0.5	1.2 ± 0.2
GRB 020531.....	GRB	PLE	17 ± 5	5.6 ± 0.7	23.0 ± 4.7	3.6 ± 0.5
GRB 020625.....	XRF	PL	2.9 ± 1.0	0.3 ± 0.2	3.2 ± 1.1	0.2 ± 0.1
GRB 020801.....	GRB	Band	6.4 ± 1.1	1.4 ± 0.3	7.7 ± 2.1	0.8 ± 0.2
GRB 020812.....	XRR	PLE	2.5 ± 0.8	0.8 ± 0.3	3.3 ± 1.0	0.5 ± 0.2
GRB 020813.....	GRB	Band	20 ± 1	13 ± 1	32 ± 2	8.3 ± 0.6
GRB 020819.....	XRR	Band	12 ± 1	5.6 ± 0.4	18 ± 1	3.4 ± 0.3
GRB 020903.....	XRF	PL	2.8 ± 0.7	$3.2^{+6.7}_{-2.4} \times 10^{-2}$	2.8 ± 0.7	$1.4^{+3.7}_{-1.1} \times 10^{-2}$
GRB 021004.....	XRR	PLE	1.8 ± 0.4	0.9 ± 0.2	2.7 ± 0.5	0.4 ± 0.2
GRB 021021.....	XRF	PL	2.1 ± 1.1	0.3 ± 0.2	2.5 ± 1.2	0.2 ± 0.2
GRB 021104.....	XRF	PLE	4.2 ± 1.8	0.7 ± 0.2	4.9 ± 1.8	0.3 ± 0.1
GRB 021112.....	XRR	PLE	3.5 ± 1.2	1.0 ± 0.4	4.5 ± 1.3	0.6 ± 0.3
GRB 021211.....	XRR	Band	22 ± 1	8.4 ± 0.6	30 ± 2	4.1 ± 0.3
GRB 030115.....	XRR	PLE	7.0 ± 1.3	1.2 ± 0.2	8.1 ± 1.4	1.2 ± 0.2
GRB 030226.....	GRB	PLE	1.7 ± 0.5	1.0 ± 0.2	2.7 ± 0.6	0.6 ± 0.1
GRB 030323.....	XRR	PL	3.4 ± 2.1	0.5 ± 0.2	3.9 ± 2.1	0.3 ± 0.2
GRB 030324.....	XRR	PLE	6.6 ± 1.0	1.6 ± 0.3	8.3 ± 1.2	1.0 ± 0.2
GRB 030328.....	GRB	Band	6.7 ± 0.5	4.9 ± 0.3	11.6 ± 0.9	3.3 ± 0.2
GRB 030329.....	XRR	Band	379 ± 21	72 ± 4	451 ± 25	38 ± 2
GRB 030416.....	XRF	PL	4.5 ± 0.9	0.3 ± 0.1	4.8 ± 0.9	$(1.4 \pm 0.6) \times 10^{-2}$
GRB 030418.....	XRR	PLE	3.7 ± 0.9	0.3 ± 0.2	4.0 ± 0.9	0.1 ± 0.1
GRB 030429.....	XRF	PLE	3.1 ± 0.7	0.7 ± 0.2	3.8 ± 0.8	0.3 ± 0.1
GRB 030519.....	GRB	Band	7.5 ± 3.4	12 ± 5	19 ± 8	8 ± 3
GRB 030528.....	XRF	Band	17.3 ± 1.5	0.6 ± 0.1	17.9 ± 1.6	$(1.5 \pm 0.6) \times 10^{-1}$
GRB 030723.....	XRF	PLE	2.0 ± 0.4	0.1 ± 0.1	2.1 ± 0.4	$3.1^{+9.4}_{-2.6} \times 10^{-2}$
GRB 030725.....	XRR	PLE	25 ± 2	9.1 ± 0.6	34 ± 2	5.7 ± 0.4
GRB 030821.....	XRR	PLE	3.8 ± 0.7	1.9 ± 0.3	5.8 ± 0.9	1.2 ± 0.2
GRB 030823.....	XRF	PLE	7.0 ± 1.6	0.6 ± 0.3	7.6 ± 1.7	0.2 ± 0.1
GRB 030824.....	XRF	PL	12 ± 4	0.3 ± 0.1	12.7 ± 3.8	$(1.3 \pm 0.7) \times 10^{-1}$
GRB 030913.....	GRB	PLE	2.2 ± 0.5	1.4 ± 0.3	3.6 ± 0.6	0.9 ± 0.2

^a GRB classification—XRF: X-ray-flash; XRR: X-ray-rich GRB; GRB: GRB.

^b Spectral model—PL: power-law; PLE: power-law times exponential cutoff; Band: Band function.

Since the attitude control camera was not operational, the celestial coordinates of GRB 010225 are not available.

In the case of the four XRRs, the normalization constants, K_{15} , of the spectra are the lowest among all of the XRRs and GRBs. We therefore interpret the lack of evidence for E_{obs} in these bursts as due to the low signal-to-noise ratio of their spectra. In these cases, it is difficult to constrain the break energy, E_0 , and a power-law model gives an adequate fit to the spectral data.

We find that a simple PL model provides an adequate fit to the spectral data for the 45 bursts in this study (six XRFs and two XRRs). In the case of the six bursts we classify as XRFs, and two XRRs), we observe that the slope of the power-law index is < -2 . We interpret this result as follows. The spectral data for these bursts do not constrain F_{peak} , but the fact that $\beta < -2$ means that we are observing the high-energy power-law portion of their Band-model spectra, and F_{obs} is near or below 2 keV, the lower limit of the WXM energy band. We therefore conclude that these are XRFs.

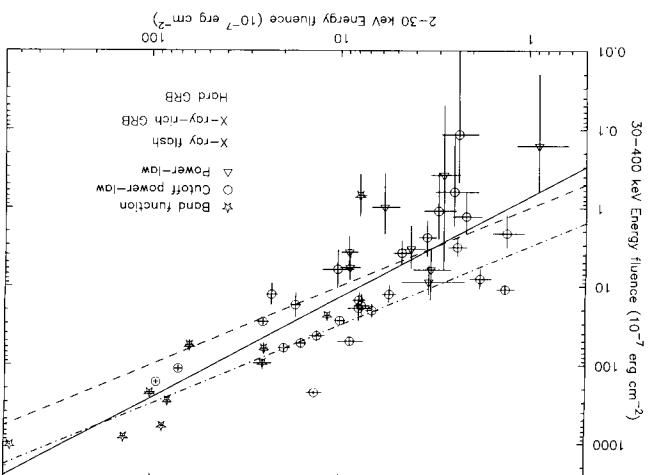
6. DISTRIBUTION OF SPECTRAL PARAMETERS

Figure 3 shows the sky distribution in ecliptic coordinates of the 44 HETE-2 XRFs, XRRs, and GRBs in this study. The HETE-2 sky coverage is not uniform, and as a result it is difficult to make a meaningful statement about the sky distributions of these three kinds of GRBs. Modulo this and the relatively small sample size of each of the three kinds of bursts, there is no statistically significant evidence that the sky distributions of the three kinds of bursts are different.

S. SKY DISTRIBUTIONS

the combination reached by Kippchen et al. (2003), who found no statistically significant evidence that the T_{50} and T_{90} distributions of *BeppeSAX* WFC XRFs and long *Compton Gamma Ray Observatory* (CGRO) BATSE bursts differ. However, we caution that the size of current *HETE-2* samples of XRFs, XRSs, and GRBs is small, as is the size of the sample of *BeppeSAX* WFC XRFs, and therefore the power of these $K-S$ tests is small.

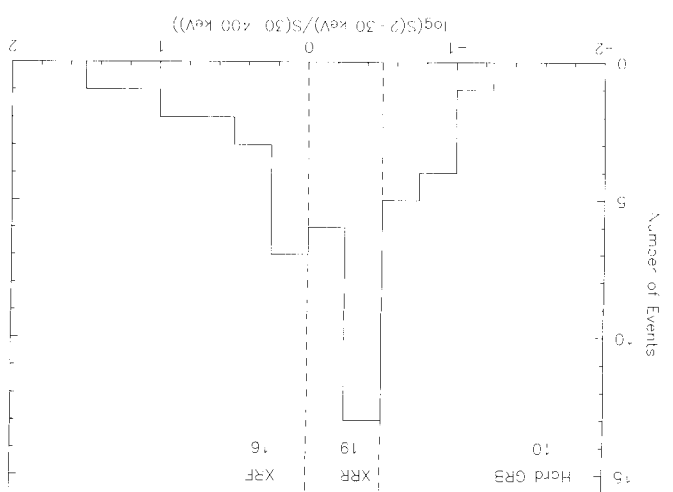
Fig. 3. Distribution of the bursts in this study in the $S_2(2-30 \text{ keV})$ - $S_4(30-400 \text{ keV})$ plane. The dashed line corresponds to the boundary between XRTs and XRAs. The dot-dashed line corresponds to the boundary between KVA and GRBs. The solid line is the best linear fit to the boundary between SFRs and GRBs. The correlation coefficient of the burst distribution is 0.851. The probability of such a correlation occurring by chance for the sample size of 45 bursts is 1.1×10^{-8} .



The distributions of the brightest peaks of GRBs show a strong dependence on the energy band in which they are measured (Fenimore et al. 1995), as does the overall duration of the bursts (Norris et al. 2000), with both $\propto E^{-0.4}$. Therefore, one might expect the T_{50} and T_{90} distributions for XRFs, XRRs, and GRBs to be different, and the T_{50} and T_{90} distributions for XRFs and XRRs to differ from those for long BATSE bursts, particularly since the durations of the latter were measured in a higher-energy band. We have used the Kolmogorov-Smirnov ($K-S$) test to investigate this possibility. Applying this test to the T_{50} distributions for XRFs and GRBs, XRRs, and XRF and XRRs, we find $K-S$ test probabilities of 0.25, 0.47, and 0.88, respectively. For the T_{90} distribution, we find $K-S$ test probabilities for the same cross-comparisons of 0.97, 0.99, and 0.91, respectively. Applying the T_{50} test to the T_{90} distributions for XRFs and XRRs, we find $K-S$ test probabilities of 0.25, 0.47, and 0.88, respectively. For the T_{90} distribution, we find $K-S$ test probabilities of 0.97, 0.99, and 0.91, respectively. Applying the T_{50} test to the T_{90} distributions for XRFs and XRRs, we find $K-S$ test probabilities of 0.66 and 0.55, respectively. For the T_{90} distribution, we find $K-S$ test probabilities of 0.74, respectively. For the T_{90} distribution, we find $K-S$ test probabilities of 0.66 and 0.55, respectively. The $K-S$ tests reveal no statistically significant evidence that the distributions for XRFs and XRRs are different, or that the distributions for T_{50} and T_{90} durations for XRFs, XRRs, and GRBs are different. The last result is consistent with those for long BATSE bursts.

4. DURATIONS

The dashed lines correspond to the borders between hard GRBs and XRBs, and between XRBs and XRFs.



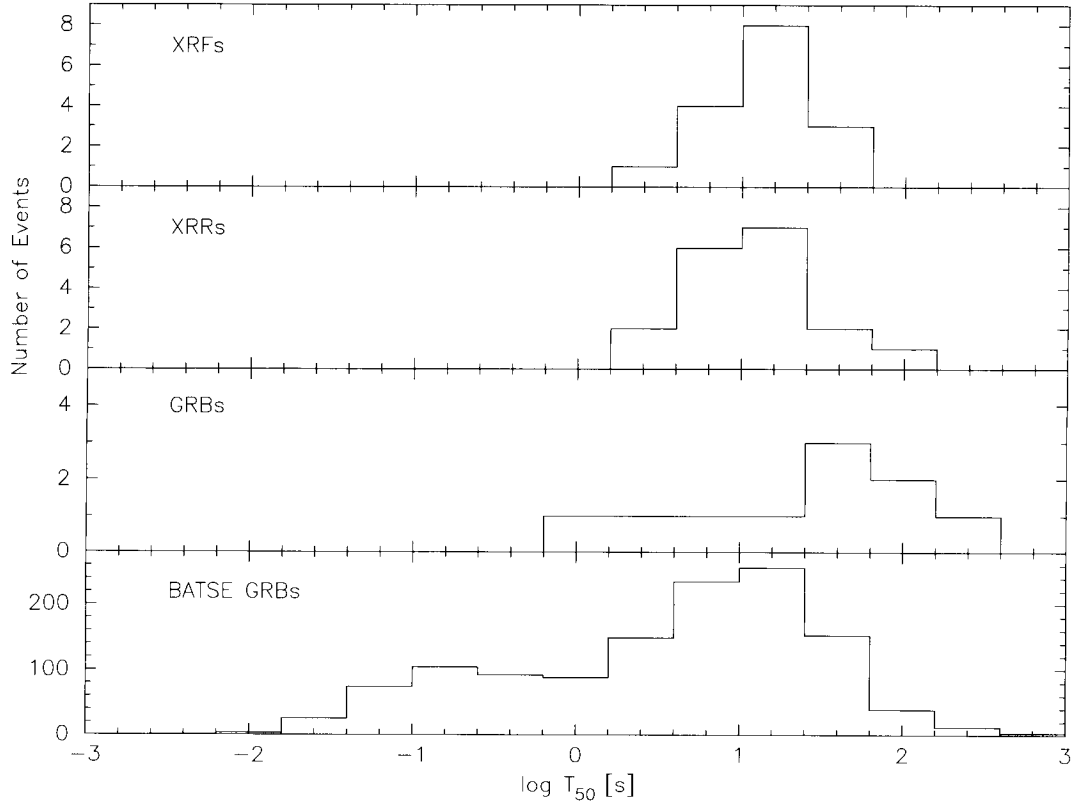


FIG. 4a

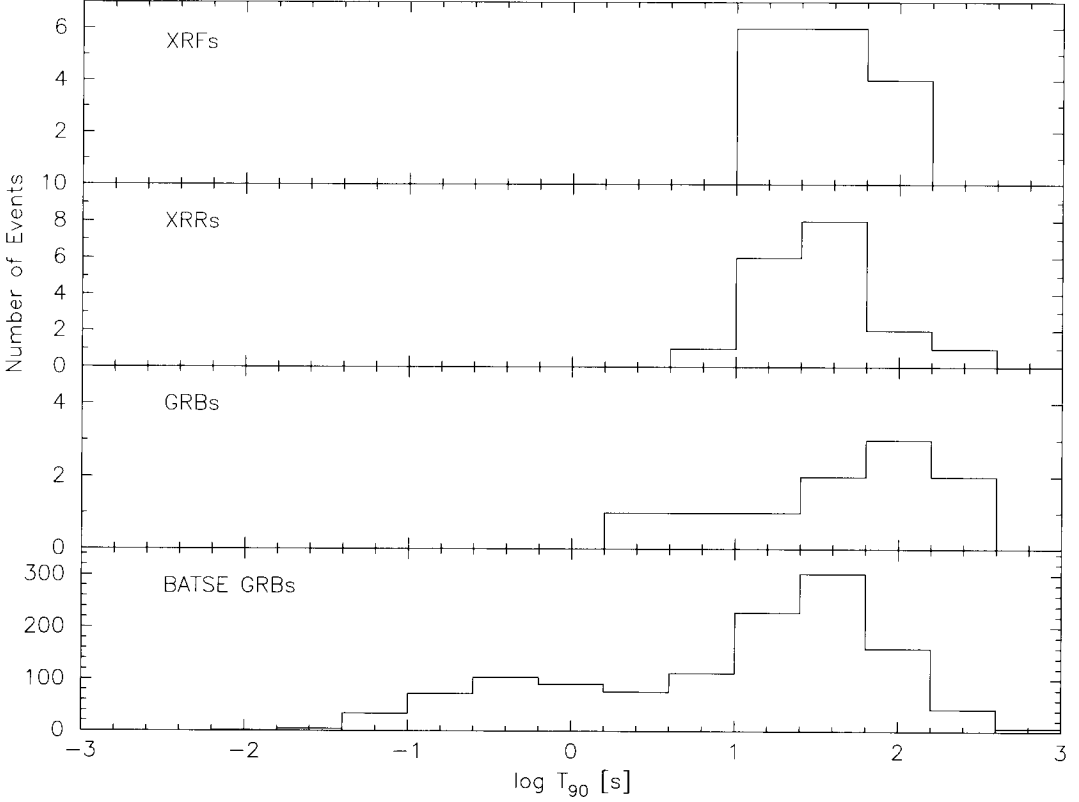


FIG. 4b

FIG. 4.—Comparison between (a) T_{50} and (b) T_{90} measures of burst duration in the 2–25 keV energy band for the three kinds of bursts seen by *HETE-2*, and in the 50–300 keV energy band for BATSE GRBs. The panels in (a) and (b) show (from top to bottom) the distribution of the durations of XRFs, XRRs, GRBs, and BATSE GRBs. The duration of the BATSE sample includes not only the long GRBs but also the short GRBs. There is no statistically significant evidence for any differences between the T_{50} and T_{90} durations of XRFs, XRRs, and GRBs, or between XRFs and long BATSE bursts (see the text for details).

There is a well-known systematic effect when fitting the PLE photon index β of the Band model. The reason for this is that the energy observations is insufficient to require the Band model: the low-energy power-law index α is smaller (more negative) than it

Figure 6 shows the distribution of the low-energy photon index α . In this figure, we include bursts that require the PLE index α to be higher than 0.5.

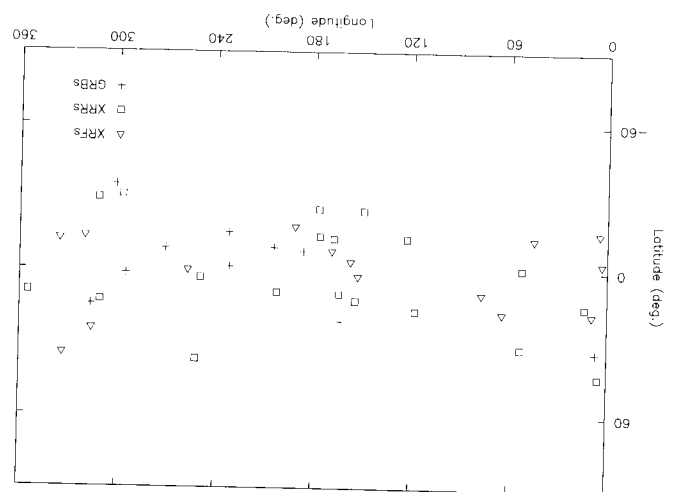
6.1. Distribution of α -Values

Table 2 gives both the χ^2 and the number of degrees of freedom (dof) for all of the spectral fits that we have done. In this table, we show with asterisks the models that are preferred at a significance $Q < 10^{-2}$ and that provide an adequate fit to the data. These are the models that we have chosen as characteristic. These are the models that we have chosen as characteristic. Tables 3, 4, and 5 give the spectral parameters for the chosen model, the photon number and photon energy fluxes in various energy bands, and the photon number number for the 45 bursts in this study.

Two of the bursts for which the Band model is preferred by XRF, five XRRs, and four GRBs) in this study. The data over the PLE model and provides an adequate fit to the spectral data have values of the high-energy power-law index $\beta > -2$ (GRBs 020813 and 030519). We do not include these two bursts in the sample of bursts whose spectral properties we now discuss, because the E_{peak} found by fitting to the HETE-2 WXM and FREGATE data lies near or above the upper limit of the FREGATE energy band and is not the actual energy of the peak of the burst spectrum in $W\text{Hz}^{-1}$. Therefore the high-energy part of the burst spectrum in the Band model that we fit to the HETE-2 data is not the actual in the Band model spectrum.

We find that the PLE model is preferred at a significance $\hat{\alpha} < 10^{-2}$ over the PL model and provides an adequate fit to the spectral data for 27 of the 45 bursts in this study (eight XRFs, 13 XRRs, and six GRBs). The Band model is preferred at a significance $\hat{\alpha} < 10^{-2}$ over the PLE model and provides an adequate fit to the spectral data for 10 of the remaining 10 bursts (one

Fig. 3. Comparison of the sky distributions in ecliptic coordinates for all of the $HETE-2$ bursts in this study.



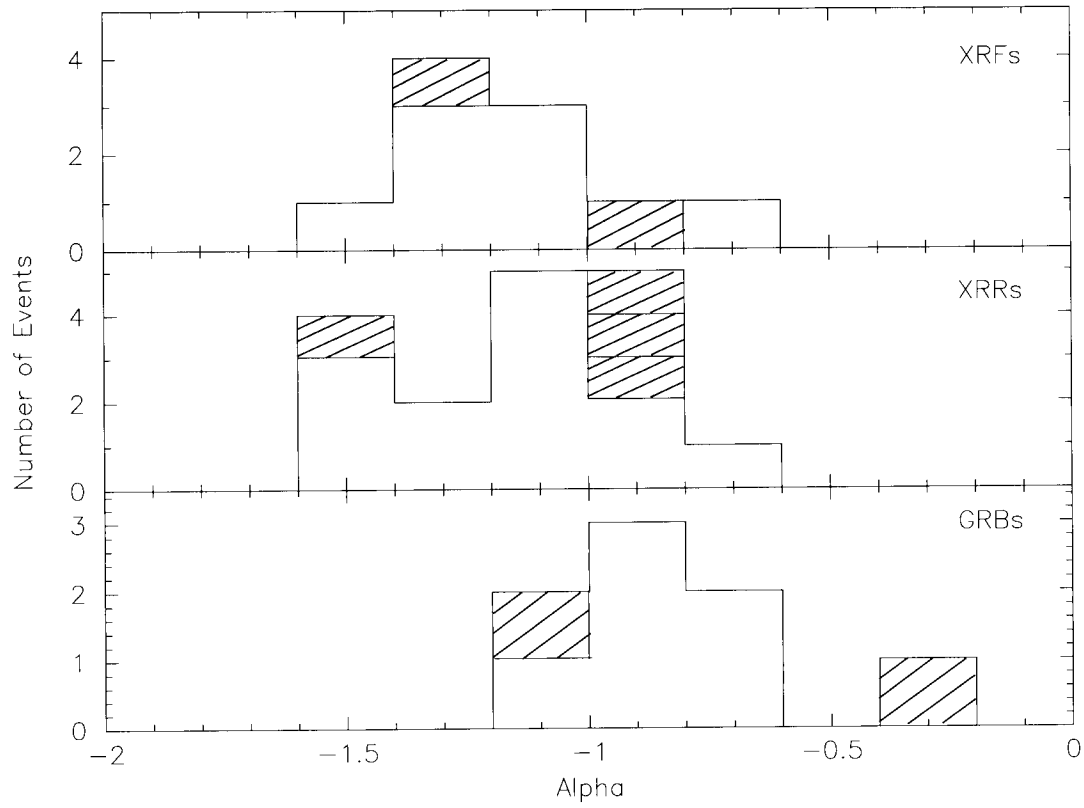


FIG. 6a

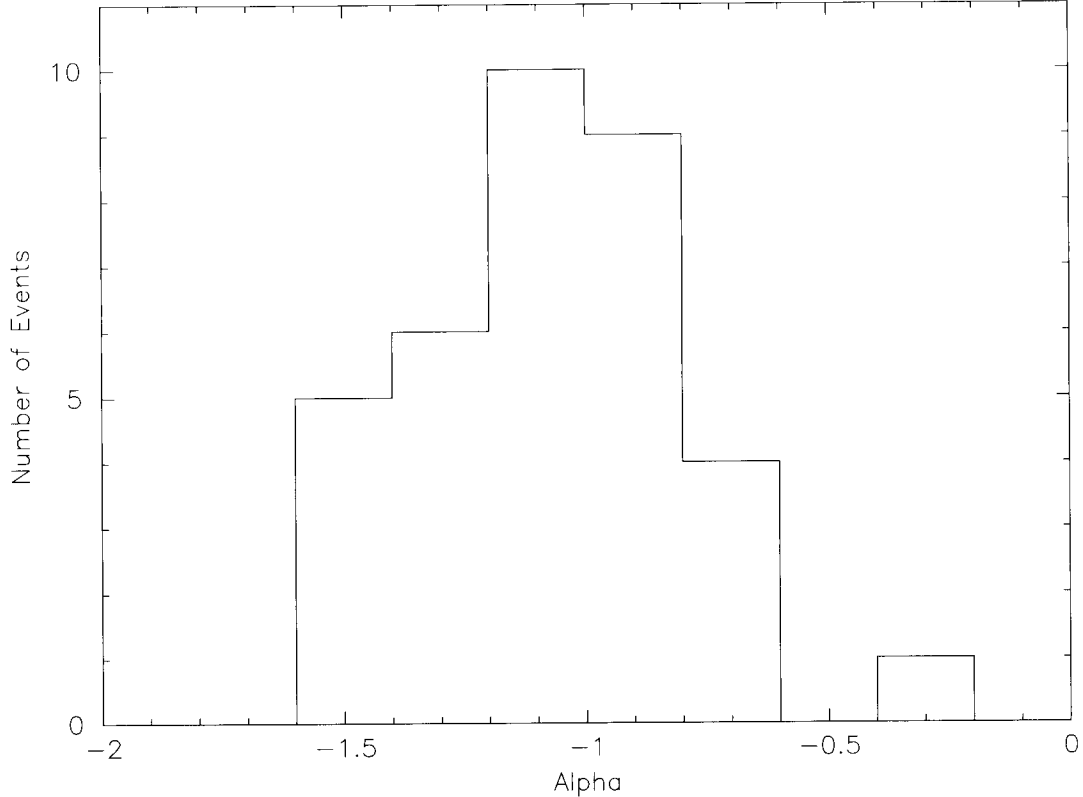
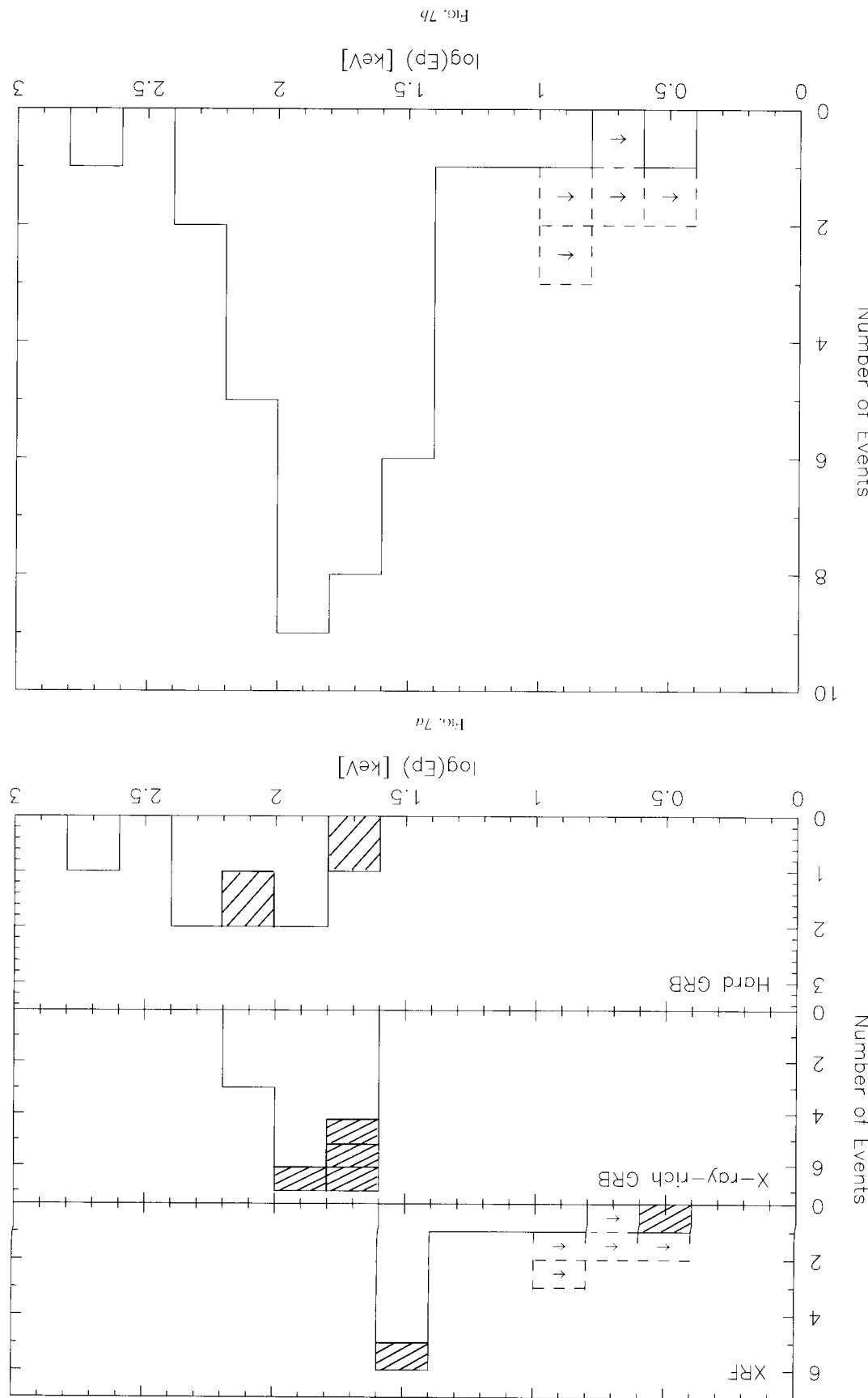


FIG. 6b

FIG. 6.— Distribution of the low-energy power-law index α for (a) each of the three kinds of bursts and (b) all of the bursts. (a) The hatched α -values are the burst spectra requiring the Band model, and the nonhatched α -values are the burst spectra that are adequately fit by the PLE model.

Fig. 7. Distribution of E_{peak} for (a) each of the three kinds of bursts and (b) all of the bursts. (a) The hatched E_{peak} values are the burst spectra requiring the Band model, and the nonhatched E_{peak} values are the burst spectra that are adequately fit by the PL-E model.



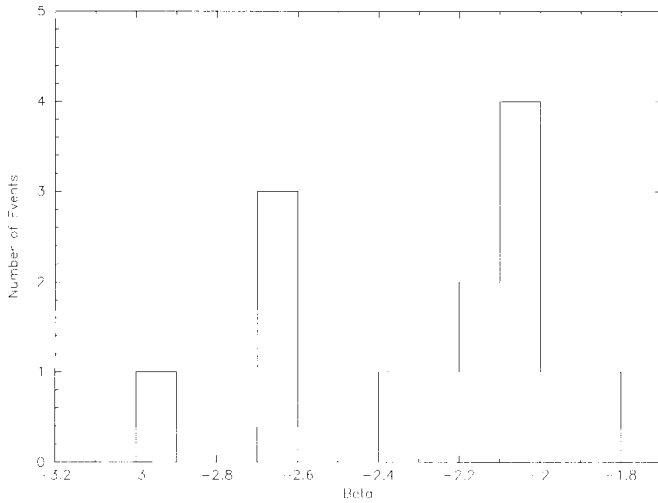


FIG. 8. Distribution of the high-energy power-law index β for all of the bursts for which β could be determined. XRF 030723 is the burst with $\beta > -2$; in the case of this burst, we can say that $\beta > -2$ with high confidence, but the actual value of β is uncertain (Butler et al. 2005). We do not include two bursts (GRBs 020813 and 030519) with $\beta > -2$ in the sample, because the $E_{\text{peak}}^{\text{obs}}$ found by fitting to the *HETE-2* WXM and FREGATE data lies near or above the upper limit of the FREGATE energy band and is not the actual energy of the peak of the burst spectrum in νF_ν . Therefore the high-energy power law in the Band model that we fit to the *HETE-2* data is not the actual β in the Band-model spectrum.

The distribution of β -values is shown in Figure 8. Because of the small number of GRBs with well-determined β -values, only the distribution for all of the GRB classes taken together is plotted. This distribution is similar to that for long BATSE bursts (Preece et al. 2000).

7. CORRELATIONS BETWEEN $E_{\text{peak}}^{\text{obs}}$ AND OTHER BURST PROPERTIES

Figure 9 shows the distribution of observed peak energy $E_{\text{peak}}^{\text{obs}}$ versus the fluence ratio $S_E(2-30 \text{ keV})/S_E(30-400 \text{ keV})$. Since the fluence ratio is independent of the normalization parameter of the model spectrum, it is possible to calculate the relationship between the fluence ratio and $E_{\text{peak}}^{\text{obs}}$. The overlaid curves in Figure 9 are the calculated relationships, assuming the Band function, for $\alpha = -1$ and $\beta = -2.5$ (red), -3.0 (blue), and -20.0 (green). The dependence of the fluence ratio on β is weak when $E_{\text{peak}}^{\text{obs}}$ is greater than 30 keV, and understandably becomes strong when $E_{\text{peak}}^{\text{obs}}$ is less than 30 keV. This implies that the choice of the proper spectral model is important for determining the fluence ratio, and for determining which bursts are XRFs and XRRs. Fortunately, the importance of choosing the correct spectral model for the latter is modest because a range in β of -2 to -20 produces a range in the fluence ratio of only 40% at $E_{\text{peak}}^{\text{obs}} = 30 \text{ keV}$, which corresponds to the boundary between XRFs and XRRs.

Figure 10 shows the distribution of α -values (*left panel*) and β -values (*right panel*) versus $E_{\text{peak}}^{\text{obs}}$. The values of α and β show no statistically significant correlation with $E_{\text{peak}}^{\text{obs}}$ and therefore none with the kind of burst. Kippen et al. (2003) also found no statistically significant correlation between α and $E_{\text{peak}}^{\text{obs}}$ in the *BeppoSAX* WFC/CGRO BATSE sample of XRFs and GRBs.

Figure 11 shows the distribution of the bursts in this study in the $[S_E(2-400 \text{ keV}), E_{\text{peak}}^{\text{obs}}]$ plane. This figure shows that there is a strong correlation between $E_{\text{peak}}^{\text{obs}}$ and $S_E(2-400 \text{ keV})$. The best-fit power-law slope between $E_{\text{peak}}^{\text{obs}}$ and $S_E(2-400 \text{ keV})$ is 0.279 ± 0.053 . The values of the slope and the uncertainty in it that we find imply a significance for the correlation of $\sim 15 \sigma$.

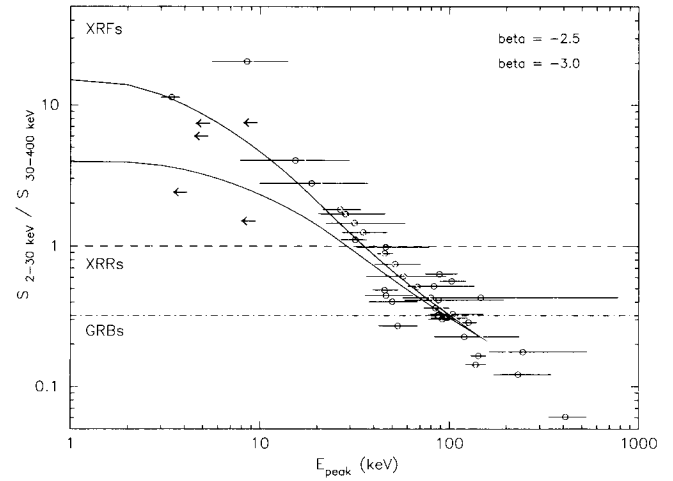


FIG. 9. Distribution of bursts in the $[E_{\text{peak}}, S_E(2-30 \text{ keV})/S_E(30-400 \text{ keV})]$ plane. Overlaid are curves corresponding to the X-ray to γ -ray fluence ratio as a function of $E_{\text{peak}}^{\text{obs}}$, assuming the Band function with $\alpha = -1$, and $\beta = -2.5$ (red), -3.0 (blue), and -20.0 (green).

The correlation coefficient of $+0.511$ that we find between the two quantities also implies a high significance for the correlation. The probability of such a correlation occurring by chance for the sample size of 40 bursts is 3.0×10^{-4} . Thus, while the scatter in the correlation is large, the significance of the correlation is also large.

Figures 12 and 13 show the distribution of *HETE-2* bursts in the $[F_N^p(2-400 \text{ keV}), E_{\text{peak}}^{\text{obs}}]$ plane and the $[F_N^p(50-300 \text{ keV}), E_{\text{peak}}^{\text{obs}}]$ plane, respectively. There is no evidence for a correlation between $E_{\text{peak}}^{\text{obs}}$ and the peak photon flux $F_N^p(2-400 \text{ keV})$, but a strong correlation exists between $E_{\text{peak}}^{\text{obs}}$ and the peak photon flux $F_N^p(50-300 \text{ keV})$. The correlation coefficient of $+0.802$ that we find between the two quantities implies a high significance for the correlation. The probability of such a correlation occurring by chance for the sample size of 40 bursts is 3.9×10^{-7} . Thus, while the scatter in the correlation is large, the significance of the correlation is also large. Kippen et al. (2003) suggested a similar correlation for the *BeppoSAX* WFC/CGRO BATSE sample of XRFs and GRBs.

However, the correlation between $E_{\text{peak}}^{\text{obs}}$ and $F_N^p(50-300 \text{ keV})$ is an artifact of the choice of 50–300 keV for the energy band in which the peak flux is measured. The reason is that for GRBs, $F_N^p(50-300 \text{ keV})$ is roughly the *bolometric* peak photon number flux, whereas for XRRs, and especially for XRFs, $F_N^p(50-300 \text{ keV})$ is clearly not the bolometric peak photon number flux. This is because $E_{\text{peak}}^{\text{obs}}$ lies near or below the lower limit of this energy band for XRRs, and far below the lower limit of the energy band for XRFs. The result is that the peak photon number fluxes for these bursts are greatly reduced from their bolometric values, as can be clearly seen by comparing Figures 12 and 13. The correlation coefficient for the distribution of bursts in the latter plane is only 0.297. Consequently, the significance of the correlation is only 94% for the sample size of 40 bursts.

Figures 14 and 15 compare the distributions of *HETE-2* bursts and *BeppoSAX* XRRs and GRBs, but not XRFs (Amati et al. 2002), in the $[S_E(2-400 \text{ keV}), E_{\text{peak}}^{\text{obs}}]$ plane and the $[F_N^p(2-400 \text{ keV}), E_{\text{peak}}^{\text{obs}}]$ plane, respectively. The distributions are similar, except that the XRFs are missing from the *BeppoSAX* distributions.

Figures 16 and 17 compare the distribution of *HETE-2* bursts in the $[F_N^p(50-300 \text{ keV}), E_{\text{peak}}^{\text{obs}}]$ plane with the distribution of

Fig. 12.—Distribution of bursts in the $[F_{\nu}(2-400 \text{ keV}), F_{\nu_{\text{peak}}}]$ plane. The correlation coefficient for the burst distribution is 0.297. The significance of the correlation is only 94%.

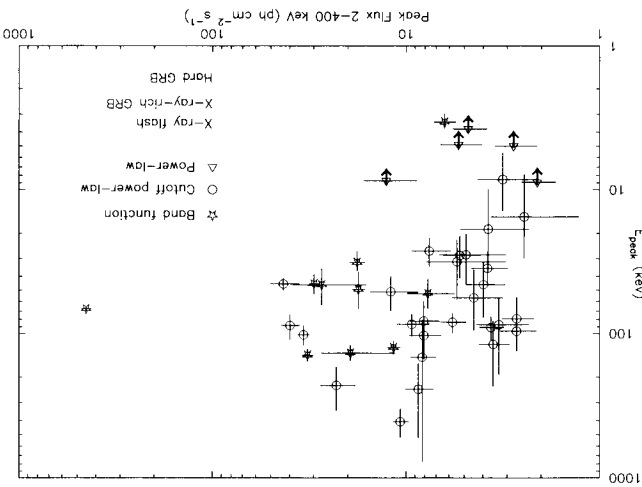


Fig. 11.—Distribution of bursts in the $[F_{\nu}(2-400 \text{ keV}), F_{\nu_{\text{peak}}}]$ plane. The solid line is the best linear fit to the burst distribution, and is given by $F_{\nu_{\text{peak}}} = (21.577 \pm 4.656) \times F_{\nu}(2-400 \text{ keV})/10^{-7} \text{ ergs cm}^{-2} \text{ s}^{-1} 2.79 \pm 0.053$. The correlation coefficient for the burst distribution is 0.511. The probability of such a correlation occurring by chance for the sample size of 40 bursts is 3.0×10^{-4} .

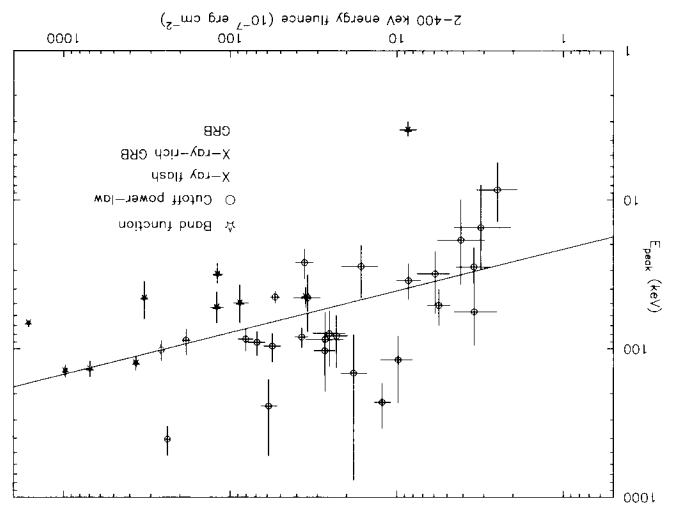


Fig. 10.—Low-energy power-law index (α) and $F_{\nu_{\text{peak}}} - F_{\nu_{\text{obs}}}$ (in $\text{erg cm}^{-2} \text{ s}^{-1}$) vs. $F_{\nu_{\text{obs}}}$. The three kinds of bursts are denoted by different colors (XRF: blue; XRB: red; and hard GRB: black), and different symbols indicate the different best-fit spectral models (PL: model; circles; band function: stars; also plotted are the XRFs for which the value of α was fixed (green)).

Fig. 10b

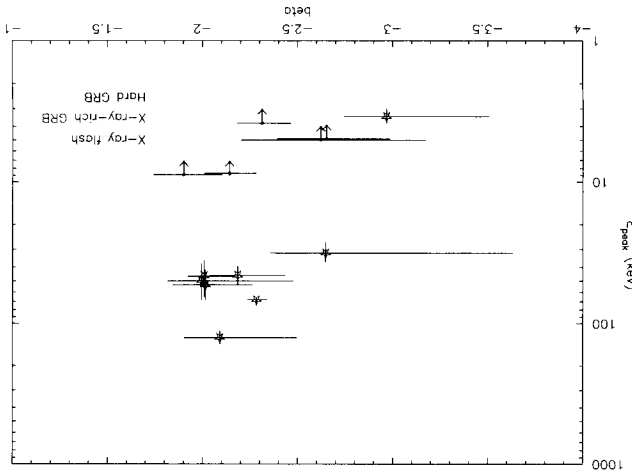
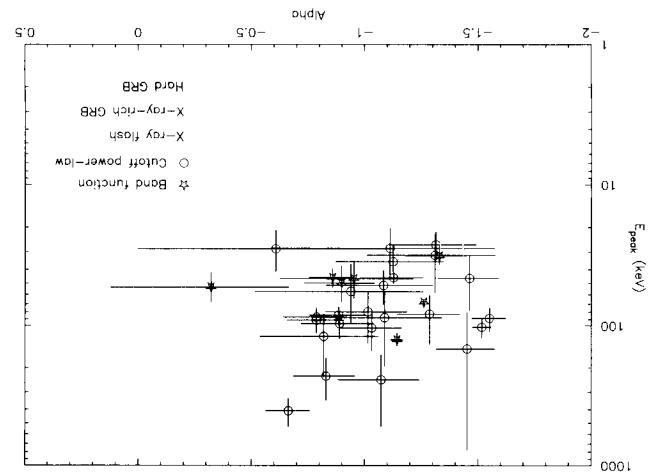


Fig. 10a



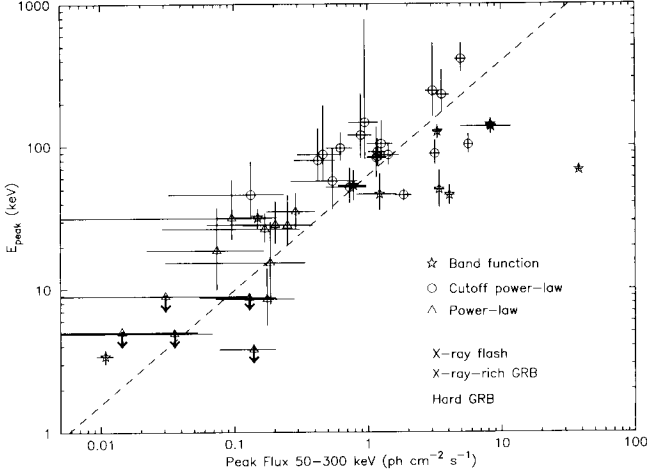


Fig. 13. Distribution of bursts in the $[F_X^P(50-300 \text{ keV}), E_{\text{peak}}^{\text{obs}}]$ plane. The dashed line corresponds to the best linear fit to the burst distribution, and is given by $E_{\text{peak}}^{\text{obs}} = (62.02 \pm 1.71) \times F_X^P(50-300 \text{ keV})^{0.80 \pm 0.32}$. The correlation coefficient for the burst distribution is 0.802. The probability of such a correlation occurring by chance for the sample size of 40 bursts is 3.9×10^{-7} .

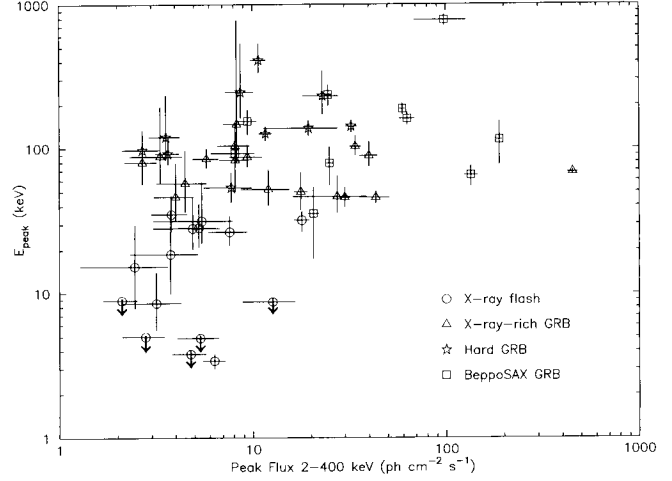


Fig. 15. Comparison of the distributions of HETE-2 bursts and BeppoSAX XRRs and GRBs, but not XRFs (Amati et al. 2002), in the $[F_X^P(2-400 \text{ keV}), E_{\text{peak}}^{\text{obs}}]$ plane. The distributions are similar, except that the XRFs are missing from the BeppoSAX distribution.

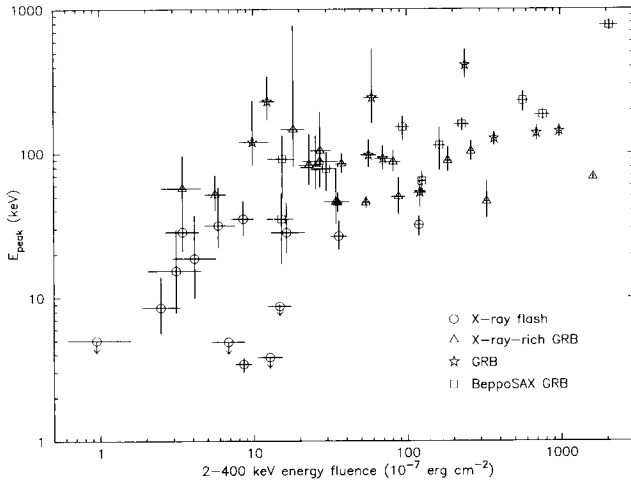


Fig. 14. Comparison of the distributions of HETE-2 bursts and BeppoSAX XRRs and GRBs, but not XRFs (Amati et al. 2002), in the $[S_L(2-400 \text{ keV}), E_{\text{peak}}^{\text{obs}}]$ plane. The distributions are similar, except that the XRFs are missing from the BeppoSAX distribution.

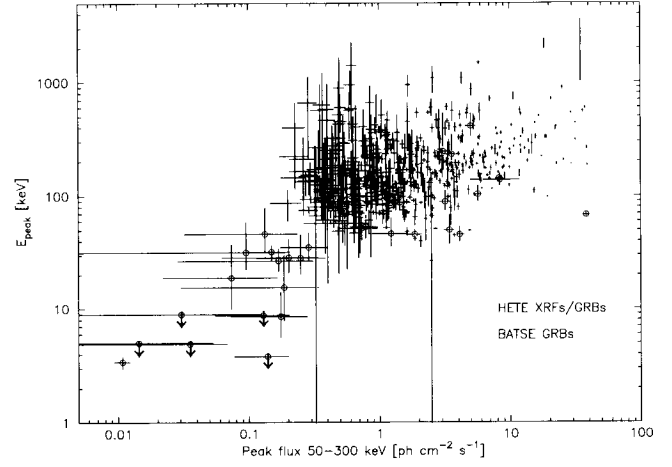


Fig. 16.---Distribution of HETE-2 bursts (black) and BATSE bursts (red) in the $[F_X^P(50-300 \text{ keV}), E_{\text{peak}}^{\text{obs}}]$ plane.

As this discussion suggests, understanding the properties of XRFs and XRSs, and clarifying the relationship between these two kinds of events and GRBs, could provide a deeper understanding of the prompt emission of GRBs. And as Lamb et al.

Lamb et al. (2005) have shown that a unified description of XRFs, XRSs, and GRBs is possible in a model in which the XRFs are due to jets with narrow opening angles, while GRBs are due to jets with wide opening angles.

If has been proposed that XRFs are due to universal GRB jets in which the luminosity falls off like a power law from the jet axis (Zhang & Meszaros 2002; Rossi et al. 2002) and are viewed well off the jet axis (Zhang et al. 2004). However, Lamb et al. (2005) have shown that such a model predicts far more XRFs than GRBs, in conflict with the HETE-2 results described in this paper. A universal GRB jet model in which the luminosity falls off per jet axis (Zhang et al. 2004; Rossi et al. 2002) and are viewed well off the jet axis (Zhang et al. 2004; Rossi et al. 2002) and are viewed well

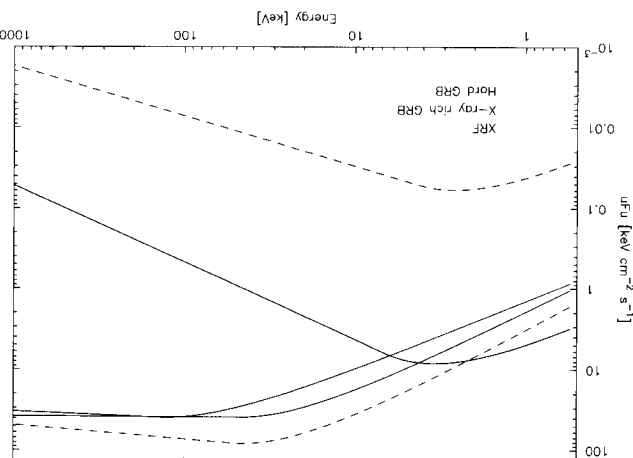
(Mochkovitch et al., 2003).

The “dirty fireball” model of XRFs posits that barion-annihilation energy is emitted in the GRB jet, resulting in a bulk Lorentz factor $\Gamma \ll 300$ (Dermer et al. 1999; Huang et al. 2002; Dermer 2003). At the opposite extreme, GRBs jets in which the bulk Lorentz factor $\Gamma \gg 300$ and the contrast between the bulk and small emission regions is also produce XRF-like events (Mormann 2003).

Yamaoka et al. (2002, 2003) have proposed that XRFs are the result of a highly collimated GRB jet vicewed well off the axis of the jet. In this model, the low values of E_{peak} and E_{iso} (and therefore of E_{obs} and S_f) seen in XRFs are the result of relativistic beaming. However, it is not clear that such a model can produce roughly equal numbers of XRFs, XRRs, and GRBs, and still satisfy the observed relation between E_{peak} and E_{iso} (Amati et al. 2002; D. Q. Lamb et al. 2002b, in preparation).

According to Melzakos et al. (2002) and Woodsley et al. (2003), X-ray (20–100 keV) photons are produced effectively by the hot cocoon surrounding the GRB jet as it breaks out, and could produce XRF-like events if viewed well off the axis of the jet. However, it is not clear that such a model would produce roughly equal numbers of XRFs, XRS, and GRBs, or the non-thermal spectral extra exhibited by XRFs.

Fig. 18. Examples of best-fit χ^2_{ν} spectra for XRTS GRB 010213 (black solid line) and GRB 020903 (black dashed line), XRTS GRB 010613 (red solid line) and GRB 021211 (red dashed line), and hard band GRB 030328 (blue solid line).



Several theoretical models of XRFs have been proposed. GRBs at very high redshifts might be observed as XRFs (Heise et al. 2001). However, the fact that the duration distribution for XRFs is similar to that for GRBs argues against this hypothesis as the explanation for most XRFs, as do the low redshifts

8.2. Theoretical Models of XRFs

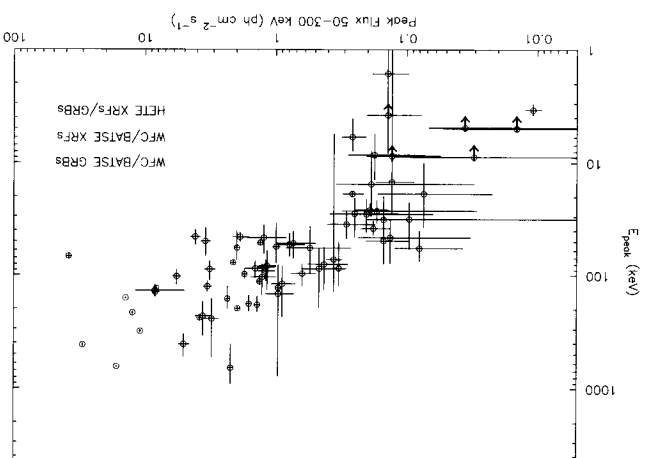
We have studied the global properties of 45 GRBs located by the *HETE-2*-WXM during the first 3 years of its mission. Using the properties of XRFs, XRRs, and GRBS, we find that the numbers of XRFs, XRRs, and GRBS are comparable for bursts occurring on the sky distributions of the three kinds of bursts. We also find that the spectral properties of XRFs and XRRs are similar to those of GRBS, except that the values of the peak energy F_{peak} of the burst spectrum in $1/\nu F_\nu$, the peak flux F_{peak} , and the fluence S_F of XRFs are much smaller and those of XRRs are smaller than those of GRBS. Figure 18, which shows the best-fit $1/\nu F_\nu$ spectra of two XRFs, two XRRs, and two GRBS, illustrates this. Our results are consistent with Barraud et al. (2003), who studied the spectral properties of the *HETE-2* GRBs using FGATH data. Finally, we find that the distributions of all three kinds of bursts form a continuum in the $(S(2-30 \text{ keV}), E_{\text{peak}})$ plane. These results provide strong evidence that all three kinds of bursts arise from the same phenomenon.

8.1. Comparison of XRF, XRR, and GRB Properties

8. DISCUSSION

long BATSE bursts (Band et al. 2004) and the distribution of WFC BATSE bursts and a representative sample of long BATSE GRBs (Kippchen et al. 2003), respectively, in the same plane. The distribution of *HE*-2 bursts is consistent with the distribution of BATSE bursts for $E_{\text{obs}} > 50 \text{ keV}$ but extends farther down in E_{obs} [and therefore in $F_p(50\text{--}300 \text{ keV})$]. This is expected because of the BATSE trigger threshold, which is 30 keV. The distribution of *HE*-2 bursts is consistent with the distribution of WFC BATSE bursts but also extends down to fainter peak fluxes for a similar reason.

Fig. 17. Distribution of W_{eff}/Z -bursts (blue) and WCF-SE bursts (red and blue) in the F_{peaks} [keV]– F_{peak} [plane].



(2005) have emphasized, XRFs may provide unique insights into the nature of GRB jets, the rate of GRBs, and the relationship between GRBs and Type Ic supernovae.

9. CONCLUSIONS

We have studied the global properties of 45 GRBs observed by *HETE*-2 during the first 3 years of its mission, focusing on the properties of XRFs and XRRs. We find that the numbers of XRFs, XRRs, and GRBs are comparable. We find that the durations and the sky distributions of XRFs and XRRs are similar to those of GRBs. We also find that the spectral properties of XRFs and XRRs are similar to those of GRBs, except that the values of the peak energy $E_{\text{peak}}^{\text{obs}}$ of the burst spectrum in νF_{ν} , the peak flux F_{peak} , and the fluence S_E of XRFs are much smaller—and those of XRRs are smaller—than those of GRBs. Finally, we find that the distributions of all three kinds of bursts form a

continuum in the [$S(2\text{--}30 \text{ keV})$, $S(30\text{--}400 \text{ keV})$] plane, the [$S(2\text{--}400 \text{ keV})$, E_{peak}] plane, and the [$F_{\text{peak}}(50\text{--}300 \text{ keV})$, $E_{\text{peak}}^{\text{obs}}$] plane. These results provide strong evidence that all three kinds of bursts arise from the same phenomenon. They also provide constraints on theoretical models of XRFs.

We would like to thank R. Marc Kippen for providing the WFC BATSE spectral parameters. We would also like to thank the anonymous referee for comments and suggestions that materially improved the paper. The *HETE* mission is supported in the US by NASA contract NASW-4690; in Japan, in part by the Ministry of Education, Culture, Sports, Science, and Technology grant-in-aid 12440063; and in France by CNES contract 793-01-8479. K. Hurley is grateful for *HETE* support under contract MIT-SC-R-293291.

REFERENCES

- Amati, L., et al. 2002, *A&A*, 390, 81
 Atteia, J-L, et al. 2003, in AIP Conf. Proc. 662, Gamma-Ray Burst and Afterglow Astronomy, ed. G. R. Ricker & R. Vanderspek (New York: AIP), 17
 Band, D. L., Norris, J. P., & Bonnell, J. T. 2004, *ApJ*, 613, 484
 Band, D. L., et al. 1993, *ApJ*, 413, 281
 Barraud, C., et al. 2003, *A&A*, 400, 1021
 Bloom, J. S., et al. 2003, *ApJ*, 599, 957
 Butler, N. R., et al. 2005, *ApJ*, 621, 884
 Dermer, C. D., Chiang, J., & Böttcher, M. 1999, *ApJ*, 513, 656
 Dermer, C. D., & Mitman, K. F. 2003, in ASP Conf. Ser. 312, Third Rome Workshop on Gamma-Ray Bursts in the Afterglow Era, ed. M. Feroci et al. (San Francisco: ASP), 301
 Fenimore, E. E., in't Zand, J. J. M., Norris, J. P., Bonnel, J. T., & Nemiroff, R. J. 1995, *ApJ*, 448, L101
 Fynbo, J. P. U., et al. 2004, *ApJ*, 609, 962
 Heise, J., in't Zand, J., Kippen, R. M., & Woods, P. M. 2001, in Gamma-Ray Bursts in the Afterglow Era, ed. E. Costa, F. Frontera, & J. Hjorth (Berlin: Springer), 16
 Huang, Y. F., Dai, Z. G., & Lu, T. 2002, *MNRAS*, 332, 735
 Kawai, N., et al. 2003, in AIP Conf. Proc. 662, Gamma-Ray Bursts and Afterglow Astronomy 2001, ed. G. R. Ricker & R. Vanderspek (New York: AIP), 25
 Kippen, R. M., Woods, P. M., Heise, J., in't Zand, J., Briggs, M. S., & Preece, R. D. 2003, in AIP Conf. Proc. 662, Gamma-Ray Bursts and Afterglow Astronomy 2001, ed. G. R. Ricker & R. Vanderspek (New York: AIP), 244
 Lamb, D. Q., Donaghy, T. Q., & Graziani, C. 2005, *ApJ*, 620, 355
 Mallozzi, R. S., Paciesas, W. S., Pendleton, G. N., Briggs, M. S., Preece, R. D., Meegan, C. A., & Fishman, G. J. 1995, *ApJ*, 454, 597
 Mészáros, P., Ramirez-Ruiz, E., Rees, M. J., & Zhang, B. 2002, *ApJ*, 578, 812
 Mochkovitch, R., Daigne, F., Barraud, C., & Atteia, J. L. 2003, in ASP Conf. Ser. 312, Third Rome Workshop on Gamma-Ray Bursts in the Afterglow Era, ed. M. Feroci et al. (San Francisco: ASP), 381
 Norris, J. P., Marani, G. F., & Bonnell, J. T. 2000, *ApJ*, 534, 248
 Olive, J.-F., et al. 2003, in AIP Conf. Proc. 662, Gamma-Ray Bursts and Afterglow Astronomy 2001, ed. G. R. Ricker & R. Vanderspek (New York: AIP), 88
 Paciesas, W. S., et al. 1999, *ApJS*, 122, 465
 Preece, R. D., Briggs, M. S., Mallozzi, R. S., Pendleton, G. N., & Paciesas, W. S. 2000, *ApJS*, 126, 19
 Rossi, E., Lazzati, D., & Rees, M. J. 2002, *MNRAS*, 332, 945
 Sakamoto, T., et al. 2004, *ApJ*, 602, 875
 Shirasaki, Y., et al. 2003, *PASJ*, 55, 1033
 Soderberg, A. M., et al. 2004, *ApJ*, 606, 994
 Woosley, S. E., Zhang, W., & Heger, A. 2003, in AIP Conf. Proc. 662, Gamma-Ray Bursts and Afterglow Astronomy 2001, ed. G. R. Ricker & R. Vanderspek (New York: AIP), 185
 Yamazaki, R., Ioka, K., & Nakamura, T. 2002, *ApJ*, 571, L31
 . 2003, *ApJ*, 593, 941
 Zhang, B., Dai, X., Lloyd-Ronning, N. M., & Mészáros, P. 2004, *ApJ*, 601, L119
 Zhang, B., & Mészáros, P. 2002, *ApJ*, 571, 876